Wind-driven sediment exchange between the Indian marginal seas over the last 18,000 years

Xiaoying Kang[a, e], Zhaojie Yu[a, b, c, d]*, Lina Song[a, c]*, Christophe Colin[f], David J. Wilson[g], Zehua Song[a], Bai Su[a], Xiaojie Tang[a, e], Fengming Chang[a], Franck Bassinot[h], Shiming Wan[a]

[a] Institute of Oceanology, Chinese Academy of Sciences, Qingdao 266071, China.

[b] Laboratory for Marine Geology, Qingdao Marine Science and Technology Center, Qingdao, 266237, China.

[c] Center for Ocean Mega-Science, Chinese Academy of Sciences, Qingdao 266071, China.

[d] College of Earth Science and Engineering, Shandong University of Science and Technology, Qingdao 266590, China.

[e] University of Chinese Academy of Sciences, Beijing 100049, China

[f] Université Paris-Saclay, CNRS, GEOPS, 91405, Orsay, France.

[g] Institute of Earth and Planetary Sciences, University College London and Birkbeck, University of London, Gower Street, London, WC1E 6BT, UK.

[h] LSCE/IPSL, CEA-CNRS-UVSQ, Université Paris-Saclay, F-91191 Gif-sur-Yvette, France

*Corresponding author: yuzhaojie@qdio.ac.cn; linasong@qdio.ac.cn

Highlights:

(1) Millennial-scale fluctuations of the Indian Coastal Current over the last 18,000 years inferred from clay minerals

(2) Atmospheric circulation changes were the main factor controlling Indian Coastal Current variability

(3) Holocene variability of the Indian Coastal Current potentially linked to changes in the Indian Ocean Dipole

Abstract

The Indian Coastal Current is the only channel for material exchange between the two largest marginal seas in the northern Indian Ocean: the Bay of Bengal and the Arabian Sea. However, its past history is poorly known, limiting accurate predictions of its future changes. Here, we present a new clay mineral record from south of India supported by interpretations of model simulations to trace its variability over the last 18,000 years. Decreased smectite/(illite+chlorite) ratios during the cold intervals suggest that a stronger northeasterly wind led to a mean southward flow of the Indian Coastal Current in the Bay of Bengal. In contrast, increased smectite/(illite+chlorite) ratios during the warm intervals suggest the opposite scenario. Combining the proxy record with model simulations, we infer that atmospheric circulation changes were the main driver of the changes. Moreover, a possible link is observed between a positive Indian Ocean Dipole (IOD) and weakened southward flow of the Indian Coastal Current in the Bay of Bengal during the Holocene. These findings imply that future warming scenarios, if associated with more intense positive IOD events as proposed, may lead to a reduction in fresh water transport from the Bay of Bengal to the Arabian Sea.

Key words: Northern Indian Ocean, Indian Coastal Current, Clay minerals, TraCE-21 model, iTraCE model

1. Introduction

The Bay of Bengal and the Arabian Sea can only connect through the ocean channel at the southern tip of the South Asian Continent, where material exchange can occur. Such exchange depends mainly on the boundary currents: the East Indian Coastal Current (EICC) in the Bay of Bengal and the West Indian Coastal Current (WICC) in the Arabian Sea, both of which reverse seasonally (Schott & McCreary Jr, 2001) (Fig. 1a), linked to the strong biannual reversal of monsoon winds. The Arabian Sea is more saline due to strong evaporation, while the Bay of Bengal is less saline due to strong precipitation and freshwater input from its surrounding rivers (Prasad, 1997; Subramanian, 1993), so changes in the EICC and WICC play an important role in the salinity budgets of the two basins. Notably, long-distance transport of clay minerals ($<$ 2 μm) by ocean currents over thousands of kilometers has been observed in a range of settings, including the western Pacific Ocean (Dang et al., 2020; Wu et al., 2012) and the South China Sea (Liu et al., 2010), as well as the Bay of Bengal (Liu et al., 2019; Yu et al., 2020) and the Arabian Sea (Phillips et al., 2014). In the western Bay of Bengal, the transport of both sediments and seawater signals from the Ganga-Brahmaputra (G-B) River system to the southern tip of India and the Arabian Sea has been demonstrated by both modern studies (Goswami et al., 2012; Prasanna Kumar et al., 2004) and palaeo-reconstructions (Chauhan & Gujar, 1996; Liu et al., 2019), indicating that the mineralogy and geochemistry of clays provide tools for tracing such currents in the past.

The seasonal changes of the Indian monsoon winds reverse the EICC (WICC) (Dandapat et al., 2018), with the southward (northward) flow occurring during the winter monsoon (Fig. 1c cf. Fig. 1b). In terms of the seasonal dynamics, the modern seasonal timing of the strongest monsoon does not completely coincide with the timing of the strongest currents (Dandapat et al., 2018). These slight discrepancies between the EICC/WICC and local winds are due to Ekman pumping, coastal Kelvin waves, and remote forcing from the equator during specific periods (McCreary et al., 1996; Mukherjee et al., 2014; Mukhopadhyay et al., 2017; Shankar et al., 1996). Nevertheless, wind forcing is the primary source of the seasonal variability in the large-scale ocean circulation and the seasonal reversals of boundary currents in the north Indian Ocean (Rao et al., 2010; Shankar et al., 2002; Suryanarayana et al., 1993). Research efforts to date have mostly focused on modern features of the EICC/WICC, such as their roles in tropical air-sea interaction (Patnaik et al., 2014), their seasonal variability (Das et al., 2020; Sen et al., 2022), and their contributions to material exchange between the Bay of Bengal and the Arabian Sea (Varna et al., 2021; Zhu et al., 2022). However, their long-term history is less well known, limiting predictions of their future evolution.

The Indian Ocean Walker circulation has a long-term average westerly wind band over the equatorial Indian Ocean (Mohtadi et al., 2017), but both the intensity and location of the westerly wind band are influenced by the Indian Ocean Dipole (IOD) (Mohtadi et al., 2017). A positive IOD is characterised by anomalous cooling of the equatorial eastern Indian Ocean, associated with an enhanced equatorial easterly wind anomaly, while a negative IOD indicates the opposite scenario (Saji et al., 1999). Previous studies showed that a positive IOD can enhance the modern Indian summer monsoon (ISM) (Anil et al., 2016; Ashok & Saji, 2007) and reduce the southward migration of the Intertropical Convergence Zone (ITCZ) (Kurniadi et al., 2021; Weller et al., 2014), whereas a negative IOD weakens the ISM and enhances the southward ITCZ migration. The observed interannual link between the ISM and the IOD might also persist on millennial and centennial timescales (Abram et al., 2009), but this link requires verification. In addition, reconstructions of the IOD over the last 1 ka from coral records reveal significant variability, as well as a trend towards a more frequent positive IOD in the last few decades (Abram et al., 2020), while climate simulations suggest that a global warming of 1.5°C will result in a positive IOD occurring twice as often as during the pre-industrial period (Cai et al., 2018). Therefore, further studies are needed to explore the detailed influence of the IOD on regional and global climate systems.

In this study, we present new clay mineral data from core MD77-191 offshore of the southern tip of the South Asian Continent (Fig. 1a) to assess changes in the sediment provenance and hence transport by the EICC and WICC to this site over the last 18 ka. We further combine these data with TraCE-21 and iTraCE simulations to explore the dynamics driving past variability of the EICC and the WICC.

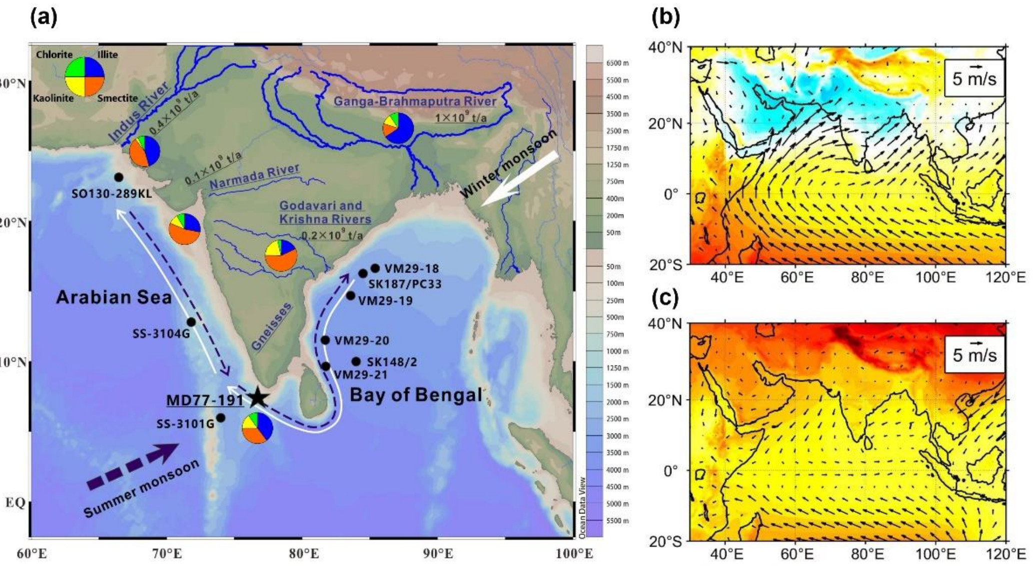

Fig. 1 (a) Bathymetric map showing the location of core MD77-191 (black star) and other cores: SO130-289KL (Deplazes et al., 2013), SS-3101G and SS-3104G (Goswami et al., 2012), VM29-18 to 21 (Colin et al., 1999), SK187/PC33 (Tripathy et al., 2011), and SK148/2 (Kessarkar et al., 2005) (black circles). Arrows show the schematic directions of the winter and summer monsoons, and the EICC and WICC (white solid line, winter; purple dashed line, summer). Pie charts show the clay mineral content of the Indus River (Alizai et al., 2012; Kessarkar et al., 2003), Ganga-Brahmaputra River (Heroy et al., 2003; Khan et al., 2019; Sarin et al., 1989), western Indian Peninsula rivers (Kessarkar et al., 2003), and the Godavari and Krishna rivers on the eastern Indian Peninsula (Bejugam & Nayak, 2016), as well as the mean data from core MD77-191 (this study). The discharges of the main rivers are also labelled (Alagarsamy & Zhang, 2005; Milliman et al., 1984; Milliman & Syvitski, 1992; Milliman & Farnsworth, 2013). (b and c) Mean distributions of the European Centre for Medium-Range Weather Forecasts reanalysis of 10-m wind (arrows) and sea level pressure (colour shading) over the northern Indian Ocean during 1979-2018 (Hersbach et al., 2020) for (b) summer (June to August), and (c) winter (December to February).

2. Materials and methods

2.1. Sediment core and age model

Core MD77-191 (7°30′ N, 76°43′ E, Fig. 1a) was collected at a water depth of 1254 m and approximately 100 km offshore of the southern tip of the South Asian Continent, during cruise OSIRIS III of the *R.V. Marion Dufresne* in 1977. Its age model was established previously using linear interpolation between 13 accelerator mass spectrometry ^{14}C dates (Bassinot et al., 2011; Ma et al., 2020) (Fig. S1). Based on this chronology, core MD77-191 spans the last ~18 ka, with linear sedimentation rates ranging from 14 to 89 cm/kyr, with a mean of 48 cm/kyr (Fig. S1).

2.2. Clay mineralogy measurements

Clay mineral analyses were conducted on 392 samples from core MD77-191 spanning the last 18 ka, with an average sample resolution of ~45 years. First, samples were treated with 15% hydrogen peroxide solution to remove organic matter, and with 20% acetic acid solution to remove inorganic carbonates. Then, the sediment was washed 4-5 times with deionised water, and the clay fraction (grain size < 2μm) was separated from the detrital sediments according to Stokes' law. The clay mineral compositions were determined by X-ray diffraction (XRD), using a D8 ADVANCE diffractometer with CuKα radiation at IOCAS. Oriented mounts of the non-calcareous clay-sized (< 2 μm) particles were analyzed (Wan et al., 2012). The Jade 6.5 software was used to semi-quantitatively obtain the relative content of the clay minerals, with an uncertainty better than 5% (2SD).

Combined Sr-Nd isotopes, and to a lesser extent clay mineralogy, are extensively used as robust tracers of sediment sources and transport processes (Kessarkar et al., 2003; Li et al., 2018). For core MD77-191, Sr-Nd isotopes were previously analysed on the clay-sized detrital fraction (< 2 μm), which minimises grain-size effects, such that provenance is the main driver of variations (Yu et al., 2022).

2.3. Transient Climate Evolution modelling

The Transient Climate Evolution (TraCE-21) model is a fully-coupled, non-accelerated atmosphere-ocean-sea ice-land surface simulation of the last 21 ka completed using the CCSM3 (Collins et al., 2006; Liu et al., 2009). This model allows the investigation of coupled atmosphere-ocean-sea ice-land surface interactions in the climate system. The iTraCE simulations are performed in the iCESM1.3, with realistic forcings applied in the time range from 21 ka to 11 ka before present (He, 2021; He et al., 2021). The iTraCE model contains 4 simulations: (1) ice sheets, greenhouse gases, orbital insolation, and meltwater fluxes, all forcing runs; (2) factorised-forcing runs with ice sheets, greenhouse gases, and orbital forcing; (3) factorised-forcing runs with ice sheets and orbital forcing; and (4) factorised runs with only ice sheet forcing. We note that the resolution of the TraCE-21 model (3.75° latitude-longitude resolution) (Collins et al., 2006; Liu et al., 2009) is lower than the iTraCE model (atmosphere and ocean model resolution are nominally 2° and 1°, respectively) (He, 2021; He et al., 2021). However, the time span of the TraCE-21 model is longer than the iTraCE model, so the two models are complementary.

In this study, we used the output from these two models to simulate upper-ocean currents, surface winds, and sea level pressure in the South Asian continental and marine areas during the intervals of Heinrich Stadial 1 (HS1: 18-14.7 ka), the Bølling-Allerød (B/A: 14.7-12.9 ka), the Younger Dryas (YD: 12.5-11.5 ka), the early Holocene (EH: 10-8 ka), and the late Holocene (LH: 2-0 ka), for summer, winter, and the annual mean (Fig. S3 to S10). The datasets used are the monthly and annual outputs from the full-forcing, which are available at https://www.cgd.ucar.edu/ccr/TraCE/ and https://www.earthsystemgrid.org/dataset/ucar.cgd.ccsm4.iTRACE.html.

3. Results and Discussion

3.1. Clay mineral sources in core MD77-191

It is difficult to distinguish sediment provenance in core MD77-191 using Sr-Nd isotopes alone, because some of the potential end members are very similar and cannot be effectively distinguished (Fig. 2a). The Sr-Nd isotopic compositions of core MD77-191 overlap with the compositions of the G-B River system and the eastern Indian Peninsula rivers, but could theoretically also be explained by a mixture of sediments from the Indus River and the western/southern Indian Peninsula rivers (Fig. 2a). Several VM and SK cores located in the western Bay of Bengal were also suggested to derive their sediment mainly from the G-B River system and the eastern Indian Peninsula rivers (Colin et al., 1999; Goswami et al., 2012; Kessarkar et al., 2005; Tripathy et al., 2011) (Fig. 1a and 2a). In addition, sediment transported from the Bay of Bengal was proposed to have led to an excursion in the Sr-Nd isotopic compositions in core SS-3101G located in the southeastern Arabian Sea during the Last Glacial Maximum (Goswami et al., 2012). The Sr-Nd isotopic compositions in core MD77-191 are close to the values in core SS-3101G from the Last Glacial Maximum and in some of the cores from the western Bay of Bengal (Fig. 2a), attesting to significant sediment sources from the Bay of Bengal.

The clay mineral assemblage of core MD77-191 consists mainly of illite (14-70%, average 40%) and smectite (0-71%, average 34%), with lower kaolinite (5-40%, average 16%) and chlorite proportions (1-23%, average 10%) (Fig. S2). In general, the illite content is inversely correlated to the smectite content ($R=-0.98$, $P < 0.01$), while the illite and chlorite contents show similar patterns through time ($R=0.56$, $P < 0.01$), although with some differences in detail (Fig. S2). Given the high sedimentation rate in core MD77-191 (～48 cm/kyr), it is clear that the clays are mainly riverine-derived, while local authigenic clay formation and wind-blown dust deposition would have made negligible contributions. Combining the Sr-Nd isotopic compositions and the clay mineral data (Fig. 2), we suggest that the sediments in core MD77-191 are likely to result from the mixing of sediments from the Bay of Bengal (G-B River system and/or eastern Indian Peninsula rivers) and the Arabian Sea (Indus River system and/or western Indian Peninsula rivers).

The smectite content in core MD77-191 was generally higher during the warm Holocene and the B/A periods (Fig. 2b, Fig. S2), which corresponds to sediment sources from the Arabian Sea. Hence, we consider that smectite was derived mainly from the Arabian Sea side, such as from the western Indian Peninsula rivers and/or the Indus River (Fig. 2b). In contrast, the higher illite and chlorite content in core MD77-191 during the cold YD and HS1 intervals (Fig. 2b, Fig. S2) indicates a trend towards the composition of clays in the G-B River system, suggesting their derivation from the Bay of Bengal side (Fig. 2b). Although the eastern Indian Peninsula rivers also supply smectite (Fig. 2b), those sediments can only be transported to core MD77-191 by southward flow of the EICC driven by the winter monsoon (Fig. 1a). In contrast, core MD77-191 had a very low smectite content during the intervals with a strong winter monsoon, such as HS1 and the YD (Fig. S2 and Fig. 2b), which does not support a major role for inputs from the eastern Indian Peninsula rivers. Additionally, although

Sri Lanka and the southern Indian Peninsula (Peninsular Gneisses) are geographically closer to the core site, these regions have lower river runoff, and their Sr-Nd isotopes and clay mineral compositions are distinct from the MD77-191 sediments (Fig. 2). Specifically, the average clay mineral composition for the southern Indian Peninsula is 73% smectite, 8% illite, 1% chlorite, and 18% kaolinite (Mascarenhas-Pereira et al., 2023), whereas the MD77-191 sediments average 34% smectite, 40% illite, 10% chlorite, and 16% kaolinite. Therefore, we consider their contributions may also be an almost continuous, but minor, background input.

Overall, the smectite/(illite+chlorite) ratios in core MD77-191 are an effective indicator of changes through time in the sediment sources to the core site (Fig. 2b, Fig. 3a) and could be used to represent the material exchange history between the Bay of Bengal and the Arabian Sea during the last deglacial and Holocene intervals. Specifically, during the warm Holocene (11.7-0 ka) and B/A (14.7-12.9 ka) periods, a strong summer monsoon could drive a southward flow of the WICC that transported more sediments from the Arabian Sea, but restricted sediment transport from the Bay of Bengal to core MD77-191 (Fig. 1). Conversely, during the cold YD (12.9-11.7 ka) and HS1 (18-14.7 ka) periods, the opposite scenario could have occurred, with strong southward flow of the EICC driving sediment export from the Bay of Bengal to core MD77-191.

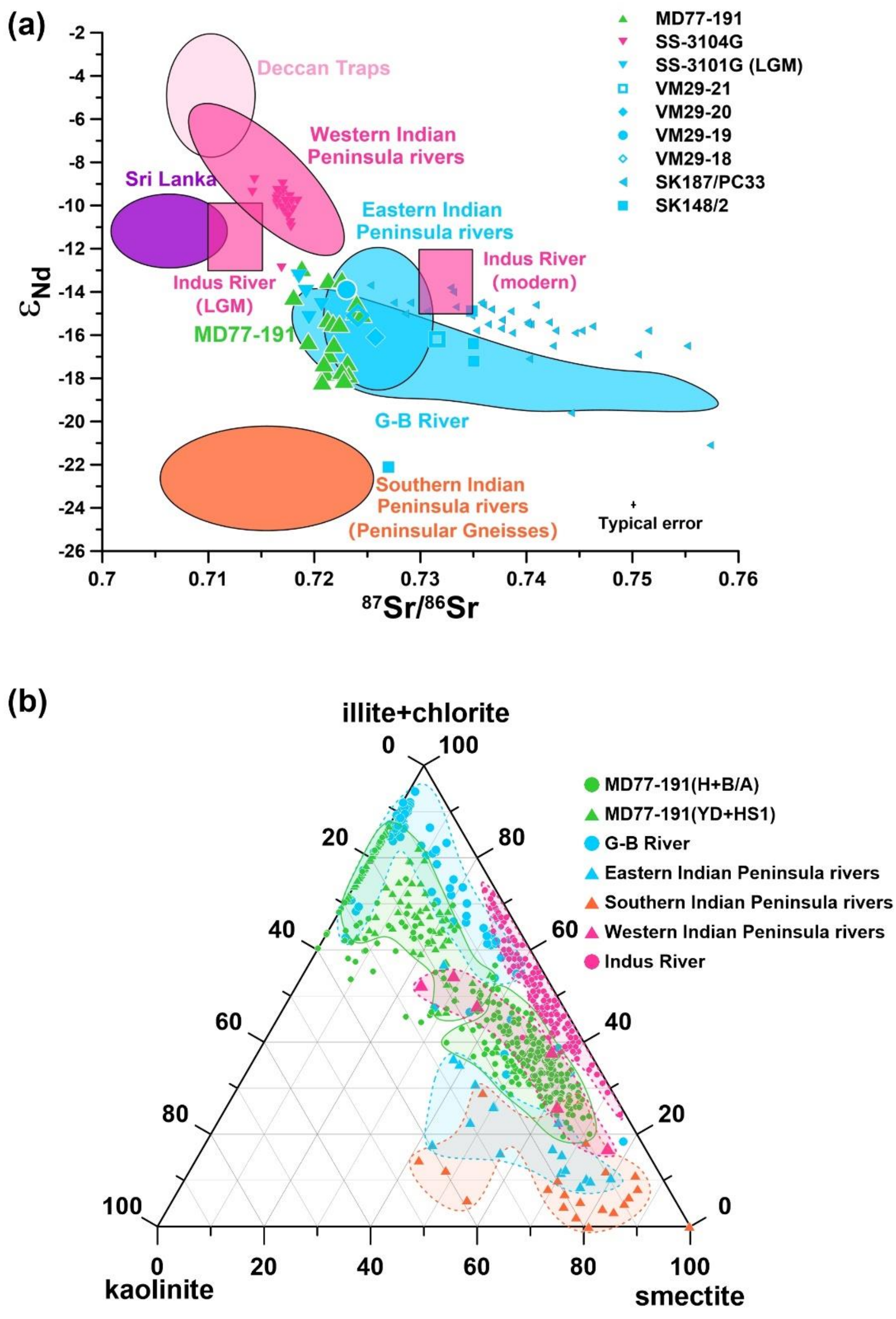

Fig. 2 (a) ε_{Nd} versus $^{87}Sr/^{86}Sr$ cross plot for Holocene and deglacial sediments from core MD77-191 (Yu et al., 2022). These data are compared to potential sources (shaded fields): Sri Lanka (Perera & Kagami, 2011), Deccan Traps (Dessert et al., 2001; Lightfoot & Hawkesworth, 1988), eastern Indian Peninsula rivers (mainly Godavari and Krishna rivers) (Ahmad et al., 2009), Ganga-Brahmaputra (G-B) River (Lupker et al., 2013; Singh & France-Lanord, 2002), Indus River (Clift et al., 2008; Clift et al., 2010; Kessarkar et al., 2003; Yu et al., 2019), western Indian Peninsula rivers (Goswami et al., 2012), and southern Indian Peninsula rivers (no data available, so based on its source region:

Peninsular Gneisses) (Goswami et al., 2012). They are also compared to data from other sediment cores (symbols): SS-3101G (Last Glacial Maximum, LGM) and SS-3104G (Goswami et al., 2012), VM29-18 to 21 (Colin et al., 1999), SK187/PC33 (Tripathy et al., 2011), and SK148/2 (Kessarkar et al., 2005). (b) Smectite-(illite+chlorite)-kaolinite ternary diagram, showing clay mineral assemblages in core MD77-191 (green dots and triangles; this study) compared to the G-B River system (blue dots) (Heroy et al., 2003; Khan et al., 2019; Sarin et al., 1989), eastern Indian Peninsula rivers (Godavari and Krishna; blue triangles) (Bejugam & Nayak, 2016), southern Indian Peninsula rivers (orange triangles) (Mascarenhas-Pereira et al., 2023), western Indian Peninsula rivers (pink triangles) (Kessarkar et al., 2003), and the Indus River (pink dots) (Alizai et al., 2012; Kessarkar et al., 2003).

3.2. Sediment transport to core MD77-191 by the Indian Coastal Current

There are two possible major controls on the variability in clay mineral assemblages in core MD77-191: (1) changes in riverine inputs over South Asia controlled by summer monsoon precipitation, and (2) changes in sediment transport by ocean currents from the river mouths to our study site. Previous studies suggested that during the Holocene and B/A periods, the increased ISM precipitation and the melting of Himalayan glaciers meant that the G-B River system transported more sediments from the Himalayas into the ocean (Joussain et al., 2016; Li et al., 2018; Tripathy et al., 2011). Therefore, at first glance, those findings seem inconsistent with the findings in this study, which instead show a reduced G-B River contribution at this time (Fig. 3a).

We argue that this apparent discrepancy arises because core MD77-191 is located offshore of the southern tip of the South Asian Continent, with its sediments being mainly transported from the Bay of Bengal and Arabian Sea by the EICC and WICC, respectively (Fig. 1a). Specifically, during the Holocene and B/A periods, the mean position of the ITCZ was further north (Fig. 3d), and the enhanced ISM could have led to higher precipitation (Fig. 3c). The enhanced precipitation would have increased erosion, and thereby increased riverine inputs to the ocean. Meanwhile, the strong ISM wind (Fig. 1b) could have led to a strong southward-flowing WICC (and northward-flowing EICC), thereby transporting sediments containing smectite from the Indus River and western Indian Peninsula rivers to core MD77-191, and restricting the supply of sediments containing illite and chlorite from the G-B River system (Fig. 3a). Conversely, during the YD and HS1, the southward movement of the ITCZ and the weakened ISM decreased the precipitation intensity (Fig. 3c and 3d), which would have weakened erosion and reduced riverine sediment fluxes. However, crucially, the enhanced winter monsoon during cold periods (Fig. 1c) could have driven a strong southward-flowing EICC (and northward-flowing WICC), thereby transporting more sediments containing illite and chlorite from the G-B River system and eastern Indian Peninsula rivers to core MD77-191, and preventing the supply of smectite-rich sediments from the Indus River and western Indian Peninsula rivers (Fig. 3a).

Therefore, we suggest that the Indian Coastal Current transportation, rather than the river sediment fluxes from the South Asian Continent, was the major factor controlling smectite/(illite+chlorite) ratios in core MD77-191. Hence, the ratio of smectite/(illite+chlorite) can indicate the variability of the EICC/WICC. Higher ratios indicate stronger southward-flowing WICC/northward-flowing EICC, while lower ratios indicate stronger southward-flowing EICC/northward-flowing WICC. We also note that the smectite content reached zero during some periods (e.g. HS1) (Fig. S2 and Fig. 3a), which was probably related to a very weak southward WICC at these times (Yang et al., 2023). However, the proxy is not expected to provide a quantitative measure of the EICC and/or WICC strength, due to possible non-linearities over its range, such as the above feature, as well as the potential for variable monsoon-driven sediment inputs to exert a secondary control through time.

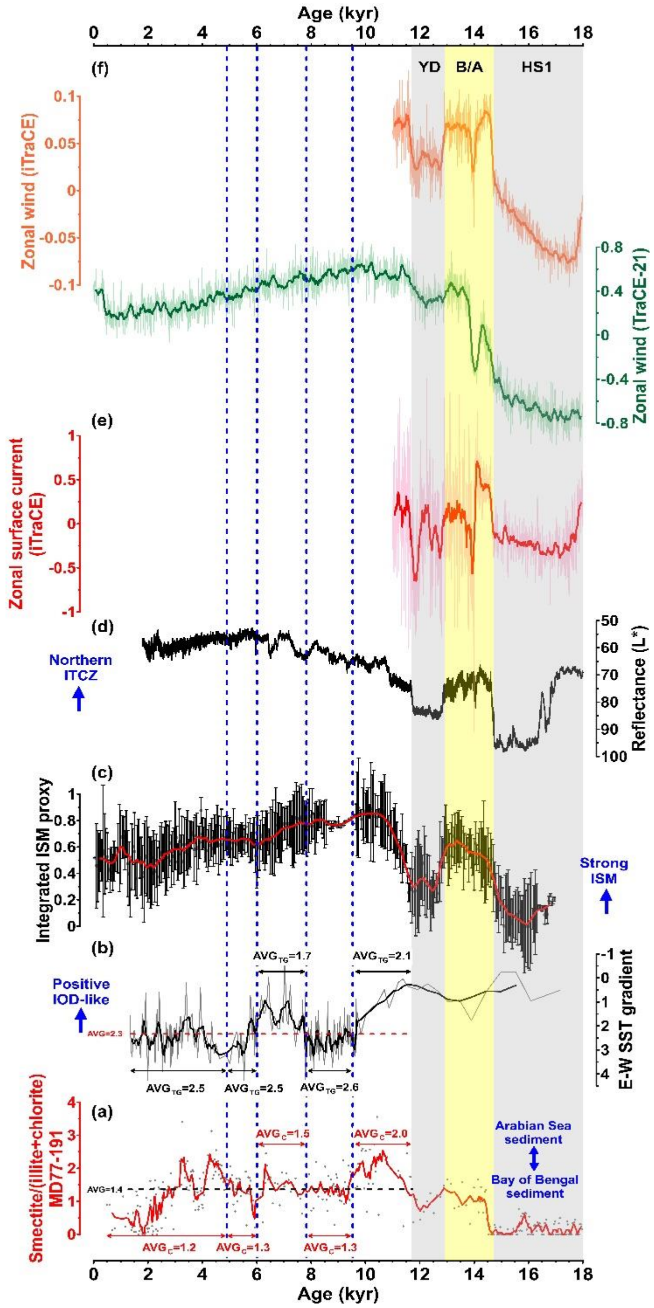

Fig. 3 Comparison of clay mineralogy in core MD77-191 to regional climate proxies. (a) Smectite/(illite+chlorite) ratio in core MD77-191 (this study). (b) Sea surface temperature (SST) gradient between the Eastern and Western Equatorial Indian Ocean (Kuhnert et al., 2014; Mohtadi et al., 2014; Romahn et al., 2014; Weldeab et al., 2022), as an indicator of the Indian Ocean Dipole (IOD). Within the Holocene, we show the average (mean) values of the SST gradient (black dashed line in panel b) and the smectite/(illite+chlorite) ratio (red dashed line in panel a). When the SST gradient is lower than the average value, it implies a positive IOD-like mode; when it is higher, it implies a negative IOD-like mode. We also show the average values of the smectite/(illite+chlorite) ratio (AVG_C) and corresponding average temperature gradient (AVG_{TG}) in the different intervals (marked by vertical blue dotted lines) to enable a quantitative comparison. (c) Integrated Indian Summer Monsoon (ISM) proxy based on stalagmite oxygen isotope records (bars show 2σ uncertainty) (Yu et al., 2022). The bold curves in (a-c) are 5-point running means. (d) Total reflectance (lightness, L*) from the Arabian Sea (Deplazes et al., 2013), which reflects the latitudinal position of the intertropical convergence zone (ITCZ). (e) Upper-ocean (100 m) zonal current anomalies in the iTraCE model near site MD77-191. (f) Comparison between TraCE-21 and iTraCE modelled mean annual zonal wind speed anomalies near site MD77-191. Only the zonal wind speeds are shown here, since these can transport material between the basins.

3.3. Indian Coastal Current changes linked to Indian Ocean atmospheric changes

While the positive IOD mode was prevalent throughout the last deglacial period, during HS1 and the YD, lower smectite/(illite+chlorite) ratios are consistent with a southward ITCZ and a weaker ISM (Fig. 3a-d). Comparatively, during the B/A period, higher smectite/(illite+chlorite) ratios coincided with a northward ITCZ and a strong ISM (Fig. 3a-d). These observations suggest that major millennial-scale fluctuations in the ISM and ITCZ jointly drove the Indian Coastal Current changes. Therefore, the

Holocene may be the key period in which the individual influences of these three factors can be better distinguished, because each of them followed a different temporal evolution (Fig. 3b-d). In addition, the potential effect of global sea level on sediment transport can be excluded as a main driver during the Holocene given that sea-level changes were modest during this interval, with sea level being relatively stable since ~8 ka (Waelbroeck et al., 2002).

During the Holocene, the long-term trends in smectite/(illite+chlorite) ratios in core MD77-191 are consistent with the variations of the ISM proxy. In contrast, the sub-millennial scale fluctuations in the smectite/(illite+chlorite) record do not correspond to changes in the ISM proxy, but are similar to the IOD proxy record. From 9.5 to 7.8 ka and from 6.0 to 4.9 ka, the negative IOD-like conditions were generally associated with lower smectite/(illite+chlorite) ratios, whereas from 11.7 to 9.5 ka and from 7.8 to 6.0 ka, the positive IOD-like conditions were generally accompanied by higher smectite/(illite+chlorite) ratios (Fig. 3a-b). There are some anomalies in the above relationship from 4.9 ka to the present, possibly because the IOD modes shifted frequently during this time. Nevertheless, the above observation implies that negative IOD conditions are associated with strengthened southward flow of the EICC and increased contributions of illite and chlorite to core MD77-191, consistent with modern studies (Dandapat et al., 2018; Sherin et al., 2018). In comparison, neither the ISM nor the ITCZ proxies show comparable millennial- to centennial-scale fluctuations during the Holocene.

We use model simulations to further explore the changes in the Indian Coastal

Current and its driving mechanisms. In the modern day, wind forcing plays an important role in driving the Indian Coastal Current (Dandapat et al., 2018; McCreary et al., 1996; Mukherjee & Kalita, 2019; Sen et al., 2022; Shankar et al., 2002). Our proxy reconstruction can be compared with the simulated annual upper-ocean current velocity and surface wind speed near core MD77-191 derived from both the TraCE-21 and iTraCE models (Fig. 3e-f). Compared to the long-term time series of TraCE-21, iTraCE only covers the deglacial interval, including the HS1, the BA, and the YD. During these three time periods, the trends of wind speed and current velocity are consistent between TraCE-21 and iTraCE, although their amplitudes are different (Fig. 3e-f, Fig. S3-S7). These results suggest that both the high-resolution iTraCE and the low-resolution TraCE-21 are capable of simulating the past atmospheric circulation in the Indian Ocean. In addition, the TraCE-21 model, with its longer time series, shows relatively stable decreasing trends in wind speed through the Holocene near core MD77-191 that are consistent with the long-term trend of smectite/(illite+chlorite) ratios (Fig. 3a, f). Owing to the high spatio-temporal resolution of the iTraCE model, the large-scale surface ocean currents it simulates in the Indian Ocean are consistent with modern summer and winter surface currents (Figures 8-9 in (Schott & McCreary Jr, 2001)). Based on the above evidence, we consider that the wind derived from the low-resolution but longer TraCE-21 model could generally be expected to represent the large-scale circulation changes during the last deglaciation.

Considering the velocity and direction of the Indian Coastal Current in the TraCE-21 model is mainly driven by the winds (Fig. 3e-f), we further used the surface winds and sea level pressure outputs (Fig. S8-S10) to calculate anomalies between time periods. Specifically, we used B/A minus HS1, and EH minus YD, to show the changes during the last deglacial transition period (Fig. 4a-d). We also used EH minus LH to reveal the changes during the more stable Holocene period (Fig. 4e-f).

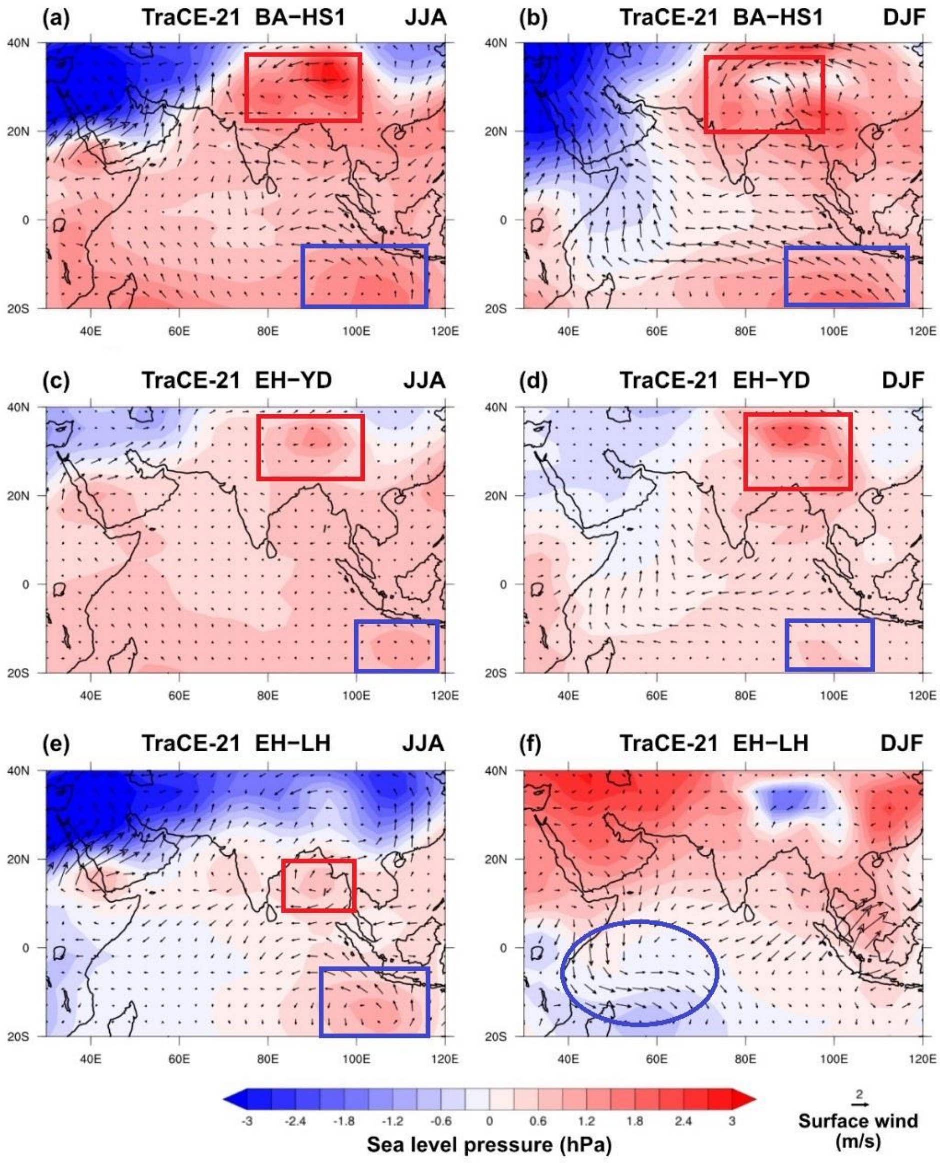

Fig. 4 Wind (arrows) and sea level pressure anomalies (colour shading) simulated in the TraCE-21 model. (a, b) Bølling-Allerød (B/A) minus Heinrich Stadial 1 (HS1) anomaly. (c, d) Early Holocene (EH) minus Younger Dryas (YD) anomaly. (e, f) Early Holocene (EH) minus late Holocene (LH) anomaly. Panels (a-c) with JJA (June, July, August) show the summer mean, and panels (d-f) with

DJF (December, January, February) show the winter mean.

The calculated anomalies comparing deglacial cold and warm states, and comparing the EH and LH, indicate two key features. Firstly, for the B/A-HS1 wind and sea level pressure anomalies, and to a lesser extent the EH-YD anomalies, during both summer and winter, there is an anticyclone anomaly in the Southern Hemisphere (blue box in Fig. 4a-d) and a cyclone anomaly on the South Asian Continent (red box in Fig. 4a-d). The anticyclone anomaly in the Southern Hemisphere could induce a southern-sourced equatorial easterly wind anomaly and a positive IOD mode, while the cyclone on the South Asian Continent could cause a prevailing southeasterly wind (stronger ISM) along the eastern coast of the Indian Peninsula. This wind could induce a mean flow into the Bay of Bengal, thereby blocking the illite and chlorite derived from the Bay of Bengal, which is consistent with higher smectite/(illite+chlorite) ratios (Fig. 3a). In contrast, for the EH-LH anomaly during summer, while the anticyclone anomaly in the Southern Hemisphere and the positive IOD mode persist (blue box in Fig. 4e), the cyclone anomaly on the South Asian Continent disappears and a new anticyclone anomaly appears in the Bay of Bengal (red box in Fig. 4e). This new anticyclone anomaly would strongly enhance the flow into the Bay of Bengal, also leading to higher smectite/(illite+chlorite) ratios as observed (Fig. 3a). For the EH-LH anomaly simulated during winter, both the wind and sea level pressure anomalies are different, with no clear cyclone/anticyclone observed in those locations (Fig. 4f).

Secondly, the wind direction over the equatorial Indian Ocean is generally the same between the simulations of the B/A-HS1, EH-YD, and EH-LH anomalies in the summer (Fig. 4a, c and e), but is reversed in the winter simulation of the EH-LH anomaly (blue ellipse in Fig. 4f). The B/A-HS1 and EH-YD anomalies during winter in the equatorial Indian Ocean exhibit easterly intensification, similar to the summer simulations, implying a positive IOD-like anomaly (Fig. 4b and d). However, this state changes to an enhanced westerly wind, particular for the western part, in the EH-LH anomaly simulated during winter, indicating a more negative IOD-like anomaly (blue ellipse in Fig. 4f). Despite the appearance of a negative IOD anomaly in winter, the enhanced smectite/(illite+chlorite) ratios for the EH compared to the LH (Fig. 3a) suggest that the positive IOD mode during summer (Fig. 3b, Fig. 4e, Fig. S9), and/or the effect of the strong ISM during the EH, dominated the sediment transport in the Indian Coastal Current.

In recent decades, more frequent and more intense positive IOD events have been observed, potentially linked to global warming and enhanced zonal sea-surface temperature gradients across the equatorial Indian Ocean (Abram et al., 2008; Cai et al., 2014). These intense positive IOD events under global warming also coincide with extreme climate variability in the tropical Indo-Pacific (Abram et al., 2020). Based on the iTrace modelling of seawater exchange between the Bay of Bengal and Arabian Sea (Fig. S11), and the past relationship between the Indian Coastal Current and the IOD observed in our study for the Holocene (Fig. 3), a more positive IOD could be expected to reduce the net fresh water inputs from the Bay of Bengal into the Arabian Sea, but it could possibly increase the intensity or variability of water exchange.

4. Conclusions

Based on clay mineral data from core MD77-191 in combination with modelling results, we reconstructed changes in sediment transport by the Indian Coastal Current and evaluated its controlling factors over the last 18 ka. During the B/A and the Holocene, a generally stronger mean southward-flowing WICC transported more smectite from the Arabian Sea, while a northward-flowing EICC restricted illite and chlorite from the Bay of Bengal, leading to higher smectite/(illite+chlorite) ratios. During HS1 and the YD, the opposite scenario occurred, with a strengthened southward-flowing EICC. The modelling results show that changes in atmospheric circulation patterns could have exerted an important control on the Indian Coastal Current flow strength and/or direction. In addition, during the Holocene, we observe a possible link between a positive IOD and a strengthened northward-flowing EICC in the Bay of Bengal. Hence, if future climate warming leads to a more frequent or stronger positive IOD state, as has been proposed, less fresh water could be transported from the Bay of Bengal to the Arabian Sea, thereby enhancing the existing salinity gradients.

Acknowledgments

This study was supported by the National Natural Science Foundation of China (42376055, 42176034 and 91958107), Strategic Priority Research Program of Chinese Academy of Sciences (XDB42010402), Natural Science Foundation of Shandong (ZR2022YQ33), Youth Innovation Promotion Association, CAS (2020210) and the National Key Research and Development Program of China (2022YFF0800503). DJW was supported by a Natural Environment Research Council independent research fellowship (NE/T011440/1). The CESM project and NCAR CISL supercomputing resources (doi:10.5065/D6RX99HX) are acknowledged for running iTraCE modelling. For the purpose of open access, the author has applied a Creative Commons Attribution (CC BY) licence to any Author Accepted Manuscript version arising.

Data Availability Statement

The data are available at Zenodo (https://zenodo.org/records/11257419).

Conflict of interest

The authors declare no competing financial or non-financial interests.

References

Abram, N. J., Gagan, M. K., Cole, J. E., Hantoro, W. S., & Mudelsee, M. (2008). Recent intensification of tropical climate variability in the Indian Ocean. *Nature Geoscience*, *1*(12), 849-853. https://doi.org/10.1038/ngeo357

Abram, N. J., McGregor, H. V., Gagan, M. K., Hantoro, W. S., & Suwargadi, B. W. (2009). Oscillations in the southern extent of the Indo-Pacific Warm Pool during the mid-Holocene. *Quaternary Science Reviews*, *28*(25-26), 2794-2803. https://doi.org/10.1016/j.quascirev.2009.07.006

Abram, N. J., Wright, N. M., Ellis, B., Dixon, B. C., Wurtzel, J. B., England, M. H., et al. (2020). Coupling of Indo-Pacific climate variability over the last millennium. *Nature*, *579*(7799), 385-392. https://doi.org/10.1038/s41586-020-2084-4

Ahmad, S. M., Padmakumari, V., & Babu, G. A. (2009). Strontium and neodymium isotopic compositions in sediments from Godavari, Krishna and Pennar rivers. *Current science*, 1766-1769. https://www.jstor.org/stable/24107258

Alagarsamy, R., & Zhang, J. (2005). Comparative studies on trace metal geochemistry in Indian and Chinese rivers. *Current science*, 299-309. https://www.jstor.org/stable/24110576

Alizai, A., Hillier, S., Clift, P. D., Giosan, L., Hurst, A., VanLaningham, S., & Macklin, M. (2012). Clay mineral variations in Holocene terrestrial sediments from the Indus Basin. *Quaternary Research*, *77*(3), 368-381. https://doi.org/10.1016/j.yqres.2012.01.008

Anil, N., Ramesh Kumar, M., Sajeev, R., & Saji, P. (2016). Role of distinct flavours of IOD events on Indian summer monsoon. *Natural Hazards*, *82*, 1317-1326. https://doi.org/10.1007/s11069-016-2245-9

Ashok, K., & Saji, N. (2007). On the impacts of ENSO and Indian Ocean dipole events on sub-regional Indian summer monsoon rainfall. *Natural Hazards*, *42*, 273-285. https://doi.org/10.1007/s11069-006-9091-0

Bassinot, F., Marzin, C., Braconnot, P., Marti, O., Mathien-Blard, E., Lombard, F., & Bopp, L. (2011).

Holocene evolution of summer winds and marine productivity in the tropical Indian Ocean in response to insolation forcing: data-model comparison. *Climate of the Past*, *7*(3), 815-829. https://doi.org/10.5194/cp-7-815-2011

Bejugam, P., & Nayak, G. (2016). Source and depositional processes of the surface sediments and their implications on productivity in recent past off Mahanadi to Pennar River mouths, western Bay of Bengal. *Palaeogeography, Palaeoclimatology, Palaeoecology*, *483*, 58-69. https://doi.org/10.1016/j.palaeo.2016.12.006

Cai, W., Santoso, A., Wang, G., Weller, E., Wu, L., Ashok, K., et al. (2014). Increased frequency of extreme Indian Ocean Dipole events due to greenhouse warming. *Nature*, *510*(7504), 254-258. https://doi.org/10.1038/nature13327

Cai, W., Wang, G., Gan, B., Wu, L., Santoso, A., Lin, X., et al. (2018). Stabilised frequency of extreme positive Indian Ocean Dipole under 1.5 C warming. *Nature communications*, *9*(1), 1419. https://doi.org/10.1038/s41467-018-03789-6

Chauhan, O. S., & Gujar, A. (1996). Surficial clay mineral distribution on the southwestern continental margin of India: evidence of input from the Bay of Bengal. *Continental Shelf Research*, *16*(3), 321-333. https://doi.org/10.1016/0278-4343(95)00015-S

Clift, P. D., Giosan, L., Blusztajn, J., Campbell, I. H., Allen, C., Pringle, M., et al. (2008). Holocene erosion of the Lesser Himalaya triggered by intensified summer monsoon. *Geology*, *36*(1), 79-82. https://doi.org/https://doi.org/10.1130/G24315A.1

Clift, P. D., Giosan, L., Carter, A., Garzanti, E., Galy, V., Tabrez, A. R., et al. (2010). Monsoon control over erosion patterns in the western Himalaya: possible feed-back into the tectonic evolution. *Geological Society, London, Special Publications*, *342*(1), 185-218. https://doi.org/10.1144/SP342.12

Colin, C., Turpin, L., Bertaux, J., Desprairies, A., & Kissel, C. (1999). Erosional history of the Himalayan and Burman ranges during the last two glacial–interglacial cycles. *Earth and Planetary Science Letters*, *171*(4), 647-660. http://ac.els-cdn.com/S0012821X99001843/1-s2.0-S0012821X99001843-main.pdf?_tid=4326d8dc-20c9-11e6-a379-00000aacb35f&acdnat=1463996127_1ccbf19a228191db33a0d2e71c228738

Collins, W. D., Bitz, C. M., Blackmon, M. L., Bonan, G. B., Bretherton, C. S., Carton, J. A., et al. (2006). The community climate system model version 3 (CCSM3). *Journal of climate*, *19*(11), 2122-2143. https://doi.org/10.1175/jcli3761.1

Dandapat, S., Chakraborty, A., & Kuttippurath, J. (2018). Interannual variability and characteristics of the East India Coastal Current associated with Indian Ocean Dipole events using a high resolution regional ocean model. *Ocean Dynamics*, *68*(10), 1321-1334. https://doi.org/10.1007/s10236-018-1201-5

Dang, H., Wu, J., Xiong, Z., Qiao, P., Li, T., & Jian, Z. (2020). Orbital and sea-level changes regulate the iron-associated sediment supplies from Papua New Guinea to the equatorial Pacific. *Quaternary Science Reviews*, *239*, 106361. https://doi.org/10.1016/j.quascirev.2020.106361

Das, B. K., Anandh, T., Kuttippurath, J., & Chakraborty, A. (2020). Influence of river discharge and tides on the summertime discontinuity of Western Boundary Current in the Bay of Bengal. *Journal of Physical Oceanography*, *50*(12), 3513-3528. https://doi.org/10.1175/JPO-D-20-0133.1

Deplazes, G., Lückge, A., Peterson, L. C., Timmermann, A., Hamann, Y., Hughen, K. A., et al. (2013). Links between tropical rainfall and North Atlantic climate during the last glacial period. *Nature Geoscience*, *6*(3), 213-217. https://doi.org/10.1038/ngeo1712

Dessert, C., Dupré, B., François, L. M., Schott, J., Gaillardet, J., Chakrapani, G., & Bajpai, S. (2001).

Erosion of Deccan Traps determined by river geochemistry: impact on the global climate and the 87Sr/86Sr ratio of seawater. *Earth and Planetary Science Letters*, *188*(3-4), 459-474. https://doi.org/10.1016/s0012-821x(01)00317-x

Goswami, V., Singh, S. K., Bhushan, R., & Rai, V. K. (2012). Temporal variations in $^{87}Sr/^{86}Sr$ and εNd in sediments of the southeastern Arabian Sea: Impact of monsoon and surface water circulation. *Geochemistry, Geophysics, Geosystems*, *13*(1).

He, C. (2021), Deciphering the deglacial evolution of water isotope and climate in the Northern Hemisphere.

He, C., Liu, Z., Otto-Bliesner, B. L., Brady, E. C., Zhu, C., Tomas, R., et al. (2021). Hydroclimate footprint of pan-Asian monsoon water isotope during the last deglaciation. *Science Advances*, *7*(4), eabe2611. https://doi.org/10.1126/sciadv.abe2611

Heroy, D. C., Kuehl, S. A., & Goodbred Jr, S. L. (2003). Mineralogy of the Ganges and Brahmaputra Rivers: implications for river switching and Late Quaternary climate change. *Sedimentary Geology*, *155*(3-4), 343-359. https://doi.org/10.1016/s0037-0738(02)00186-0

Hersbach, H., Bell, B., Berrisford, P., Hirahara, S., Horányi, A., Muñoz-Sabater, J., et al. (2020). The ERA5 global reanalysis. *Quarterly Journal of the Royal Meteorological Society*, *146*(730), 1999-2049. https://doi.org/10.1002/qj.3803

Joussain, R., Colin, C., Liu, Z., Meynadier, L., Fournier, L., Fauquembergue, K., et al. (2016). Climatic control of sediment transport from the Himalayas to the proximal NE Bengal Fan during the last glacial-interglacial cycle. *Quaternary Science Reviews*, *148*, 1-16. https://doi.org/10.1016/j.quascirev.2016.06.016

Kessarkar, P. M., Rao, V. P., Ahmad, S. M., & Babu, G. A. (2003). Clay minerals and Sr–Nd isotopes of the sediments along the western margin of India and their implication for sediment provenance. *Marine Geology*, *202*(1), 55-69. https://doi.org/https://doi.org/10.1016/S0025-3227(03)00240-8

Kessarkar, P. M., Rao, V. P., Ahmad, S., Patil, S., Kumar, A. A., Babu, G. A., et al. (2005). Changing sedimentary environment during the Late Quaternary: Sedimentological and isotopic evidence from the distal Bengal Fan. *Deep Sea Research Part I: Oceanographic Research Papers*, *52*(9), 1591-1615. https://doi.org/10.1016/j.dsr.2005.01.009

Khan, M. H. R., Liu, J., Liu, S., Seddique, A. A., Cao, L., & Rahman, A. (2019). Clay mineral compositions in surface sediments of the Ganges-Brahmaputra-Meghna river system of Bengal Basin, Bangladesh. *Marine Geology*, *412*, 27-36.

Kuhnert, H., Kuhlmann, H., Mohtadi, M., Meggers, H., Baumann, K. H., & Pätzold, J. (2014). Holocene tropical western Indian Ocean sea surface temperatures in covariation with climatic changes in the Indonesian region. *Paleoceanography*, *29*(5), 423-437. https://doi.org/10.1002/2013PA002555

Kurniadi, A., Weller, E., Min, S. K., & Seong, M. G. (2021). Independent ENSO and IOD impacts on rainfall extremes over Indonesia. *International Journal of Climatology*, *41*(6), 3640-3656. https://doi.org/https://doi.org/10.1002/joc.7040

Li, J., Liu, S., Shi, X., Zhang, H., Fang, X., Chen, M.-T., et al. (2018). Clay minerals and Sr-Nd isotopic composition of the Bay of Bengal sediments: Implications for sediment provenance and climate control since 40 ka. *Quaternary International*, *493*, 50-58. https://doi.org/10.1016/j.quaint.2018.06.044

Lightfoot, P., & Hawkesworth, C. (1988). Origin of Deccan Trap lavas: evidence from combined trace element and Sr-, Nd-and Pb-isotope studies. *Earth and Planetary Science Letters*, *91*(1-2), 89-104. https://doi.org/10.1016/0012-821x(88)90153-7

Liu, J., He, W., Cao, L., Zhu, Z., Xiang, R., Li, T., et al. (2019). Staged fine-grained sediment supply from the Himalayas to the Bengal Fan in response to climate change over the past 50,000 years. *Quaternary Science Reviews*, *212*, 164-177.

Liu, Z., Otto-Bliesner, B., He, F., Brady, E., Tomas, R., Clark, P., et al. (2009). Transient simulation of last deglaciation with a new mechanism for Bølling-Allerød warming. *science*, *325*(5938), 310-314. https://doi.org/10.1126/science.1171041

Liu, Z. F., Colin, C., Li, X. J., Zhao, Y. L., Tuo, S. T., Chen, Z., et al. (2010). Clay mineral distribution in surface sediments of the northeastern South China Sea and surrounding fluvial drainage basins: Source and transport. *Marine Geology*, *277*(1-4), 48-60. https://doi.org/10.1016/j.margeo.2010.08.010

Lupker, M., France-Lanord, C., Galy, V., Lavé, J., & Kudrass, H. (2013). Increasing chemical weathering in the Himalayan system since the Last Glacial Maximum. *Earth and Planetary Science Letters*, *365*, 243-252.

Ma, R., Sépulcre, S., Bassinot, F., Haurine, F., Tisnérat-Laborde, N., & Colin, C. (2020). North Indian Ocean Circulation Since the Last Deglaciation as Inferred From New Elemental Ratio Records for Benthic Foraminifera Hoeglundina elegans. *Paleoceanography and Paleoclimatology*, *35*. https://doi.org/10.1029/2019PA003801

Mascarenhas-Pereira, M., Nath, B. N., Neetu, S., Rebelo, R. A., Sebastian, T., Sarkar, A., et al. (2023). Modern sedimentation on the eastern continental shelf of India: Assessing the provenance and sediment dispersal pattern. *Marine Geology*, *464*, 107126. https://doi.org/https://doi.org/10.1016/j.margeo.2023.107126

McCreary, J., Han, W., Shankar, D., & Shetye, S. (1996). Dynamics of the east India coastal current: 2. Numerical solutions. *Journal of Geophysical Research: Oceans*, *101*(C6), 13993-14010. https://doi.org/10.1029/96jc00560

Milliman, J., Quraishee, G., & Beg, M. (1984). Sediment discharge from the Indus River to the ocean: past, present and future. *Marine geology and oceanography of Arabian Sea and coastal Pakistan*, 65-70.

Milliman, J. D., & Syvitski, J. P. (1992). Geomorphic/tectonic control of sediment discharge to the ocean: the importance of small mountainous rivers. *The journal of Geology*, *100*(5), 525-544. https://doi.org/https://doi.org/10.1086/629606

Milliman, J. D., & Farnsworth, K. L. (2013), *River discharge to the coastal ocean: a global synthesis*, Cambridge University Press.

Mohtadi, M., Prange, M., Schefuß, E., & Jennerjahn, T. C. (2017). Late Holocene slowdown of the Indian Ocean Walker circulation. *Nature communications*, *8*(1), 1015. https://doi.org/10.1038/s41467-017-00855-3

Mohtadi, M., Prange, M., Oppo, D. W., De Pol-Holz, R., Merkel, U., Zhang, X., et al. (2014). North Atlantic forcing of tropical Indian Ocean climate. *Nature*, *509*(7498), 76-80. https://doi.org/10.1038/nature13196

Mukherjee, A., & Kalita, B. (2019). Signature of La Niña in interannual variations of the East India Coastal Current during spring. *Climate dynamics*, *53*, 551-568.

Mukherjee, A., Shankar, D., Fernando, V., Amol, P., Aparna, S., Fernandes, R., et al. (2014). Observed seasonal and intraseasonal variability of the East India Coastal Current on the continental slope. *Journal of Earth System Science*, *123*(6), 1197-1232. https://doi.org/10.1007/s12040-014-0471-7

Mukhopadhyay, S., Shankar, D., Aparna, S., & Mukherjee, A. (2017). Observations of the sub-inertial, near-surface East India Coastal Current. *Continental Shelf Research*, *148*, 159-177.

https://doi.org/10.1016/j.csr.2017.08.020

Patnaik, K., Maneesha, K., Sadhuram, Y., Prasad, K., Ramana Murty, T., & Brahmananda Rao, V. (2014). East India Coastal Current induced eddies and their interaction with tropical storms over Bay of Bengal. *Journal of operational oceanography*, *7*(1), 58-68. https://doi.org/10.1080/1755876X.2014.11020153

Perera, L. R. K., & Kagami, H. (2011). Centimetre-and Metre-scale Nd and Sr Isotopic Homogenization in Kadugannawa Complex, Sri Lanka. *Journal of the Geological Society of Sri Lanka*, *14*, 129-141. https://www.researchgate.net/publication/235945363

Phillips, S. C., Johnson, J. E., Underwood, M. B., Guo, J., Giosan, L., & Rose, K. (2014). Long-timescale variation in bulk and clay mineral composition of Indian continental margin sediments in the Bay of Bengal, Arabian Sea, and Andaman Sea. *Marine and Petroleum Geology*, *58*, 117-138.

Prasad, T. (1997). Annual and seasonal mean buoyancy fluxes for the tropical Indian Ocean. *Current Science*, 667-674. https://www.jstor.org/stable/24100427

Prasanna Kumar, S., Narvekar, J., Kumar, A., Shaji, C., Anand, P., Sabu, P., et al. (2004). Intrusion of the Bay of Bengal water into the Arabian Sea during winter monsoon and associated chemical and biological response. *Geophysical Research Letters*, *31*(15). https://doi.org/10.1029/2004GL020247

Rao, R. R., Girish Kumar, M. S., Ravichandran, M., Rao, A. R., Gopalakrishna, V. V., & Thadathil, P. (2010). Interannual variability of Kelvin wave propagation in the wave guides of the equatorial Indian Ocean, the coastal Bay of Bengal and the southeastern Arabian Sea during 1993–2006. *Deep Sea Research Part I: Oceanographic Research Papers*, *57*(1), 1-13. https://doi.org/https://doi.org/10.1016/j.dsr.2009.10.008

Romahn, S., Mackensen, A., Groeneveld, J., & Pätzold, J. (2014). Deglacial intermediate water reorganization: New evidence from the Indian Ocean. *Climate of the Past*, *10*(1), 293-303. https://doi.org/10.5194/cp-10-293-2014

Saji, N., Goswami, B. N., Vinayachandran, P., & Yamagata, T. (1999). A dipole mode in the tropical Indian Ocean. *Nature*, *401*(6751), 360-363. https://doi.org/10.1038/43854

Sarin, M., Krishnaswami, S., Dilli, K., Somayajulu, B., & Moore, W. (1989). Major ion chemistry of the Ganga-Brahmaputra river system: weathering processes and fluxes to the Bay of Bengal. *Geochimica et cosmochimica acta*, *53*(5), 997-1009. https://doi.org/10.1016/0016-7037(89)90205-6

Schott, F. A., & McCreary Jr, J. P. (2001). The monsoon circulation of the Indian Ocean. *Progress in Oceanography*, *51*(1), 1-123. https://doi.org/10.1016/s0079-6611(01)00083-0

Sen, R., Pandey, S., Dandapat, S., Francis, P., & Chakraborty, A. (2022). A numerical study on seasonal transport variability of the North Indian Ocean boundary currents using Regional Ocean Modeling System (ROMS). *Journal of Operational Oceanography*, *15*(1), 32-51. https://doi.org/10.1080/1755876X.2020.1846266

Shankar, D., Vinayachandran, P., & Unnikrishnan, A. (2002). The monsoon currents in the north Indian Ocean. *Progress in oceanography*, *52*(1), 63-120. https://doi.org/https://doi.org/10.1016/S0079-6611(02)00024-1

Shankar, D., McCreary, J., Han, W., & Shetye, S. (1996). Dynamics of the East India Coastal Current: 1. Analytic solutions forced by interior Ekman pumping and local alongshore winds. *Journal of Geophysical Research: Oceans*, *101*(C6), 13975-13991. https://doi.org/10.1029/96JC00559

Sherin, V., Durand, F., Gopalkrishna, V., Anuvinda, S., Chaitanya, A., Bourdallé-Badie, R., & Papa, F. (2018). Signature of Indian Ocean Dipole on the western boundary current of the Bay of Bengal. *Deep Sea Research Part I: Oceanographic Research Papers*, *136*, 91-106. https://doi.org/https://doi.org/10.1016/j.dsr.2018.04.002

Singh, S. K., & France-Lanord, C. (2002). Tracing the distribution of erosion in the Brahmaputra watershed from isotopic compositions of stream sediments. *Earth and Planetary Science Letters*, *202*(3), 645-662. https://doi.org/10.1016/S0012-821X(02)00822-1

Subramanian, V. (1993). Sediment load of Indian rivers. *Current Science*, 928-930. https://www.jstor.org/stable/24096213

Suryanarayana, A., Murty, V. S. N., & Rao, D. P. (1993). Hydrography and circulation of the Bay of Bengal during early winter, 1983. *Deep Sea Research Part I: Oceanographic Research Papers*, *40*(1), 205-217. https://doi.org/https://doi.org/10.1016/0967-0637(93)90061-7

Tripathy, G. R., Singh, S. K., Bhushan, R., & Ramaswamy, V. (2011). Sr–Nd isotope composition of the Bay of Bengal sediments: Impact of climate on erosion in the Himalaya. *Geochemical Journal*, *45*(3), 175-186.

Varna, M., Singh, A., Sahoo, D., & Sengupta, D. (2021). Strengthening of Basin-Scale Ocean Currents in Winter Drives Decadal Salinity Decline in the Eastern Arabian Sea. *Geophysical Research Letters*, *48*(16), e2021GL094516. https://doi.org/10.1029/2021GL094516

Waelbroeck, C., Labeyrie, L., Michel, E., Duplessy, J.-C., Mcmanus, J. F., Lambeck, K., et al. (2002). Sea-level and deep water temperature changes derived from benthic foraminifera isotopic records. *Quaternary science reviews*, *21*(1-3), 295-305. https://doi.org/10.1016/s0277-3791(01)00101-9

Wan, S., Yu, Z., Clift, P. D., Sun, H., Li, A., & Li, T. (2012). History of Asian eolian input to the West Philippine Sea over the last one million years. *Palaeogeography, Palaeoclimatology, Palaeoecology*, *326*, 152-159. https://doi.org/10.1016/j.palaeo.2012.02.015

Weldeab, S., Rühlemann, C., Ding, Q., Khon, V., Schneider, B., & Gray, W. R. (2022). Impact of Indian Ocean surface temperature gradient reversals on the Indian Summer Monsoon. *Earth and Planetary Science Letters*, *578*, 117327. https://doi.org/https://doi.org/10.1016/j.epsl.2021.117327

Weller, E., Cai, W., Min, S.-K., Wu, L., Ashok, K., & Yamagata, T. (2014). More-frequent extreme northward shifts of eastern Indian Ocean tropical convergence under greenhouse warming. *Scientific reports*, *4*(1), 6087. https://doi.org/10.1038/srep06087

Wu, J., Liu, Z., & Zhou, C. (2012). Late Quaternary glacial cycle and precessional period of clay mineral assemblages in the Western Pacific Warm Pool. *Chinese Sci Bull*, *57*, 3748-3760. https://doi.org/10.1007/s11434-012-5277-x

Yang, Y., Zhang, L., Yi, L., Zhong, F., Lu, Z., Wan, S., et al. (2023). A contracting Intertropical Convergence Zone during the Early Heinrich Stadial 1. *Nature Communications*, *14*(1), 4695. https://doi.org/10.1038/s41467-023-40377-9

Yu, Z., Colin, C., Bassinot, F., Wan, S., & Bayon, G. (2020). Climate-Driven Weathering Shifts Between Highlands and Floodplains. *Geochemistry, Geophysics, Geosystems*, *21*(7), e2020GC008936. https://doi.org/10.1029/2020gc008936

Yu, Z., Colin, C., Wilson, D. J., Bayon, G., Song, Z., Sepulcre, S., et al. (2022). Millennial variability in intermediate ocean circulation and Indian monsoonal weathering inputs during the last deglaciation and Holocene. *Geophysical Research Letters*, *49*(21), e2022GL100003.

Yu, Z., Colin, C., Wan, S., Saraswat, R., Song, L., Xu, Z., et al. (2019). Sea level-controlled sediment transport to the eastern Arabian Sea over the past 600 kyr: Clay minerals and SrNd isotopic evidence from IODP Site U1457. *Quaternary Science Reviews*, *205*, 22-34. https://doi.org/https://doi.org/10.1016/j.quascirev.2018.12.006

Zhu, J., Zhang, Y., Cheng, X., Wang, X., Sun, Q., & Du, Y. (2022). Effect of mesoscale eddies on the transport of low-salinity water from the Bay of Bengal into the Arabian Sea during winter. *Geoscience*

Letters, *9*(1), 37. https://doi.org/10.1186/s40562-022-00246-7

Supplementary Information for

Wind-driven sediment exchange between the Indian marginal seas over the last 18,000 years

Xiaoying Kang[a, e], Zhaojie Yu[a, b, c, d]*, Lina Song[a, c]*, Christophe Colin[f], David J. Wilson[g], Zehua Song[a], Bai Su[a], Xiaojie Tang[a, e], Fengming Chang[a], Franck Bassinot[h], Shiming Wan[a]

[a] Institute of Oceanology, Chinese Academy of Sciences, Qingdao 266071, China.

[b] Laboratory for Marine Geology, Qingdao Marine Science and Technology Center, Qingdao，266237, China.

[c] Center for Ocean Mega-Science, Chinese Academy of Sciences, Qingdao 266071, China.

[d] College of Earth Science and Engineering, Shandong University of Science and Technology, Qingdao 266590, China.

[e] University of Chinese Academy of Sciences, Beijing 100049, China.

[f] Université Paris-Saclay, CNRS, GEOPS, 91405, Orsay, France.

[g] Institute of Earth and Planetary Sciences, University College London and Birkbeck, University of London, Gower Street, London, WC1E 6BT, UK.

[h] LSCE/IPSL, CEA-CNRS-UVSQ, Université Paris-Saclay, F-91191 Gif-sur-Yvette, France.

*Corresponding author: yuzhaojie@qdio.ac.cn; linasong@qdio.ac.cn

This file includes:

Figures S1 to S11

Supplementary References

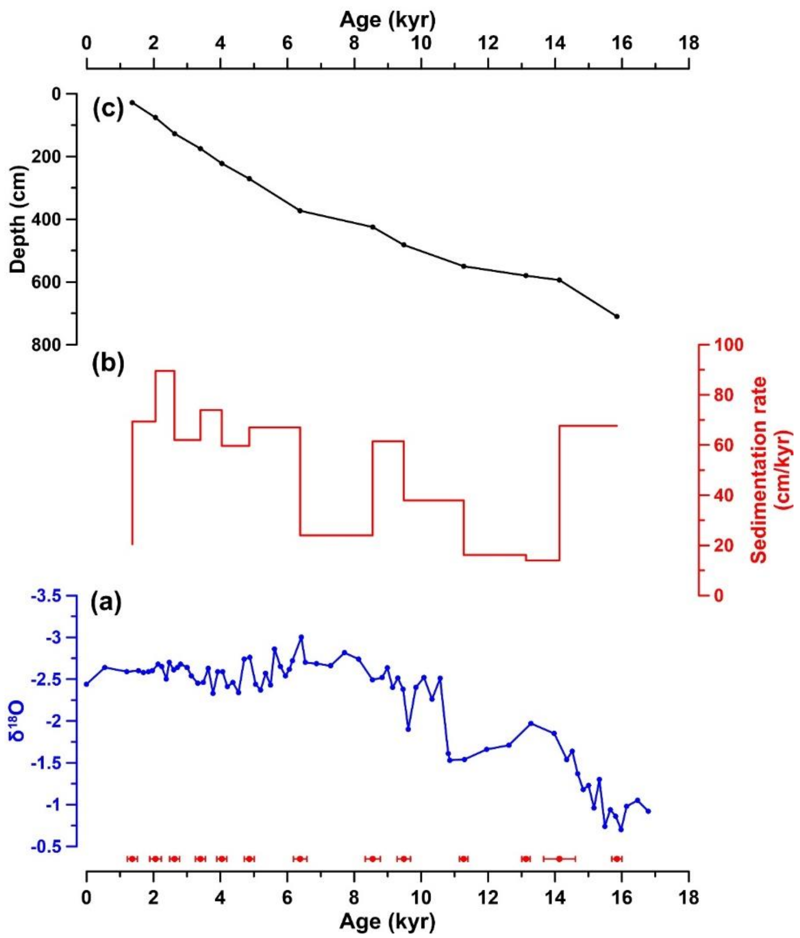

Fig. S1 (a) Planktic $\delta^{18}O$ (blue points and line) and AMS ^{14}C dating points (red points with 1σ error bars) (Bassinot et al., 2011; Ma et al., 2020); (b) sedimentation rate; (c) depth versus age in core MD77-191.

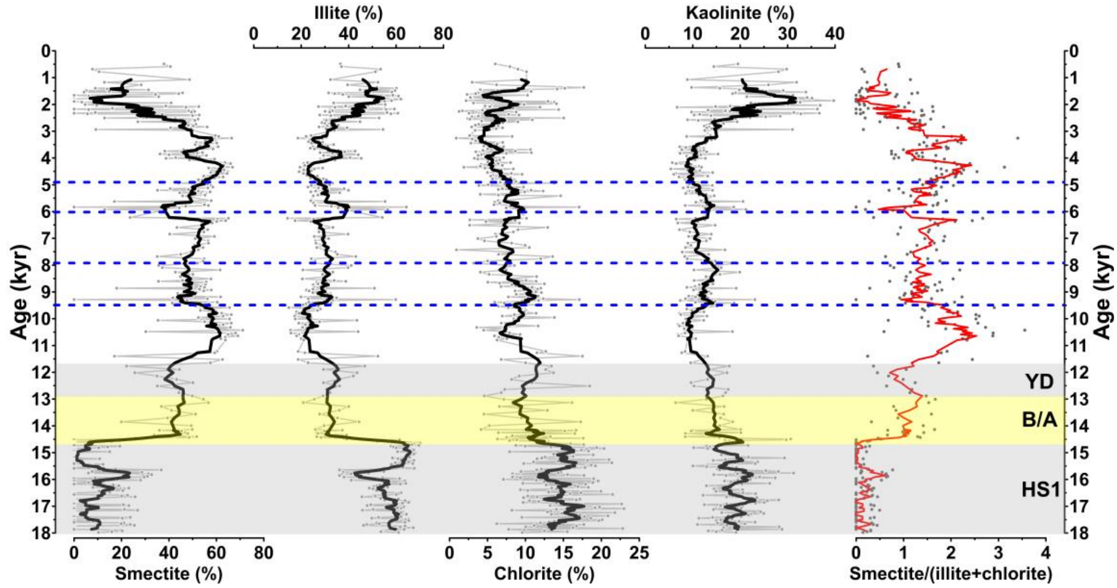

Fig. S2 Clay mineral assemblages in core MD77-191 from 0-18 ka (this study). The two grey bars indicate Heinrich Stadial 1 (HS1) and the Younger Dryas (YD), and the yellow bar indicates the Bolling-Allerod (B/A). The blue dotted lines represent excursions to lower smectite/(illite+chlorite) ratios during the Holocene. Data points and thin lines are measured data. Thick lines are 9-point (black lines) and 5-point (red line) running means.

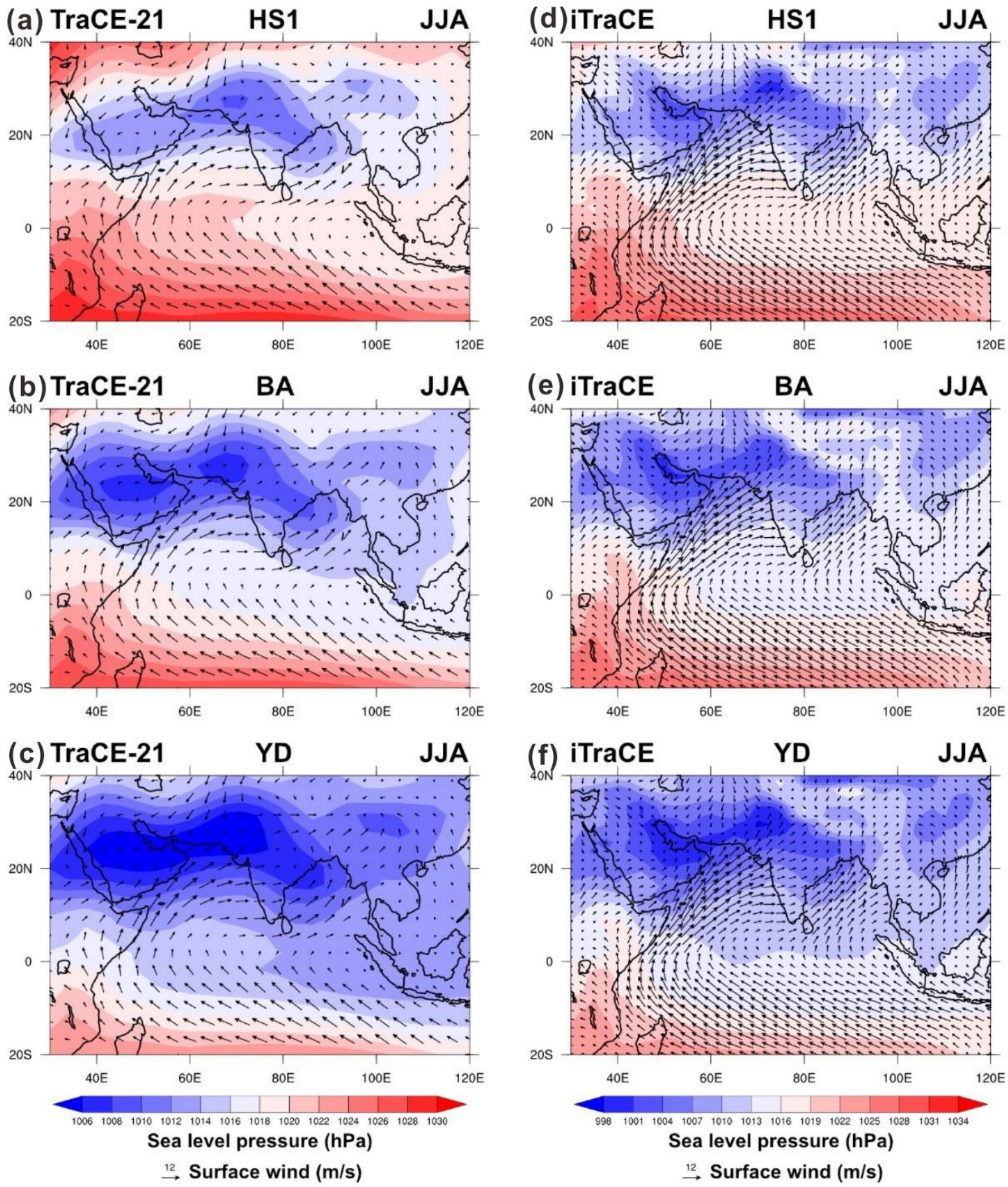

Fig. S3 Surface wind (arrows) and sea level pressure (colour shading) simulated in the TraCE-21 model for the summer (June, July, August) of (a) HS1 (18-14.7 ka), (b) BA (14.7-12.9 ka), and (c) YD (12.5-11.5 ka) (Liu et al., 2009). (d-f) are the same as (a-c) but for the iTraCE simulation (He, 2021; He et al., 2021).

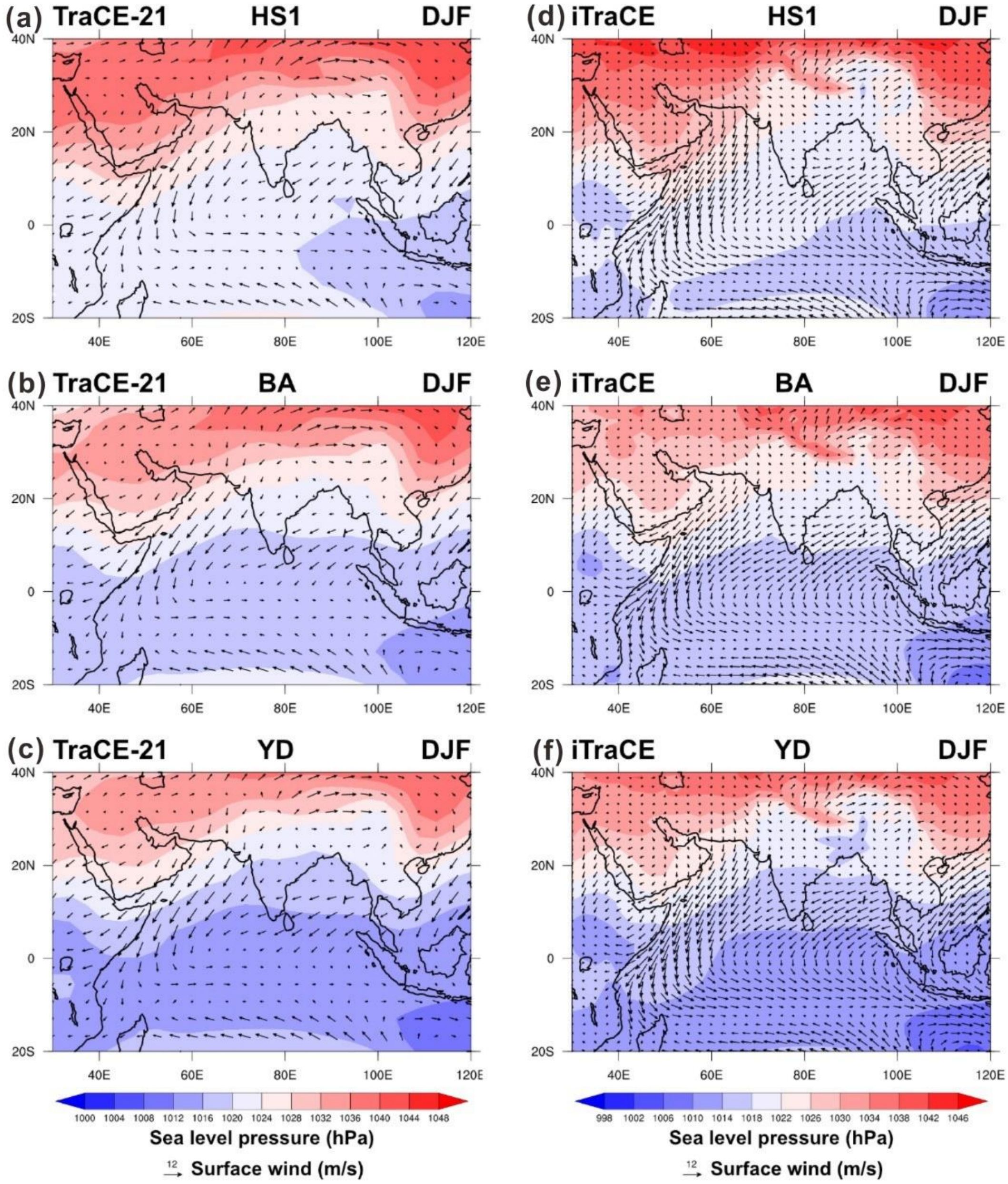

Fig. S4 The same as Fig. S3, but for winter (December, January, February) (He, 2021; He et al., 2021; Liu et al., 2009).

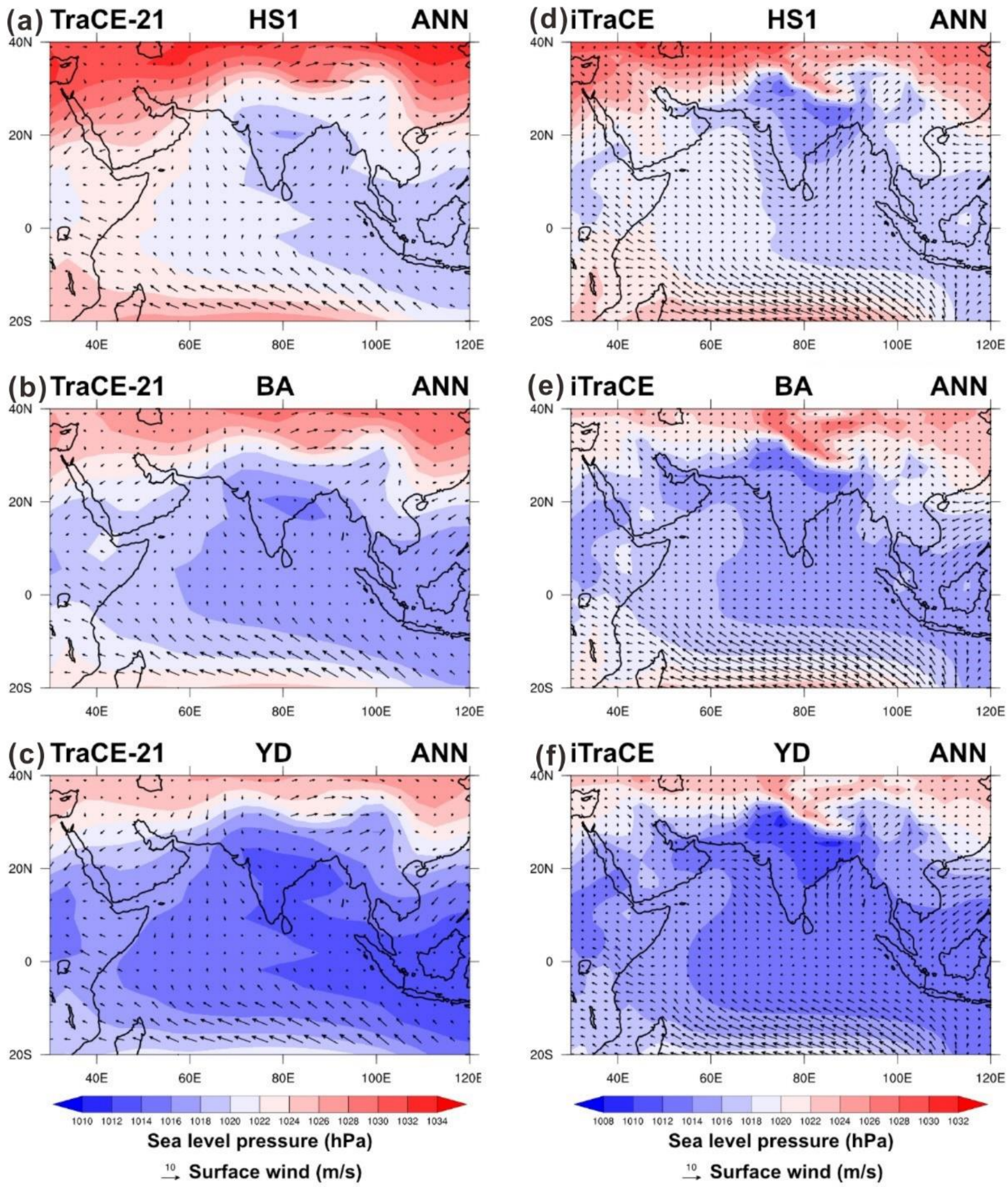

Fig. S5 The same as Fig. S3, but for the annual mean (He, 2021; He et al., 2021; Liu et al., 2009).

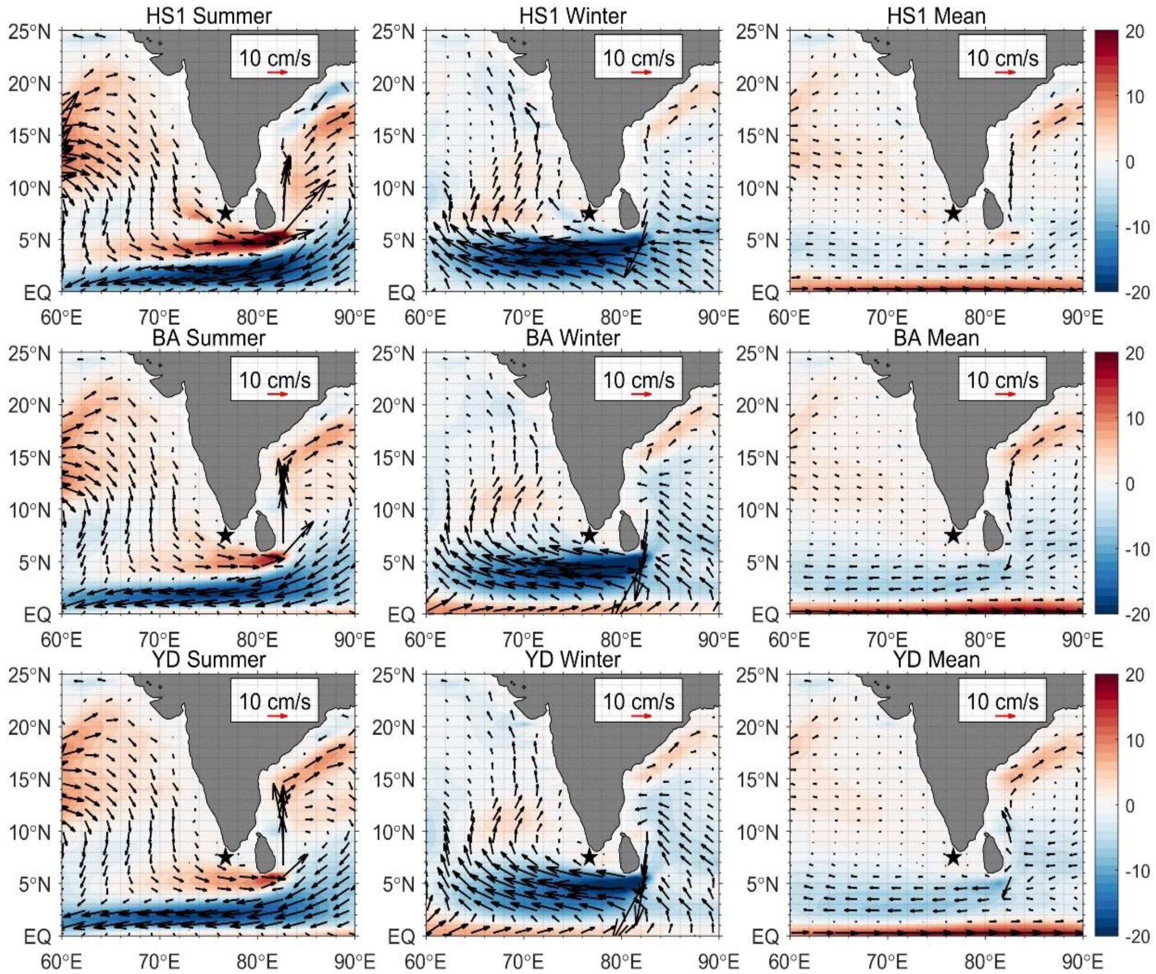

Fig. S6 Surface currents (arrows) and zonal currents (colour shading) simulated in the iTraCE model for the summer, winter, and annual mean of HS1 (18-14.7 ka), BA (14.7-12.9 ka), and YD (12.5-11.5 ka) (He, 2021; He et al., 2021).

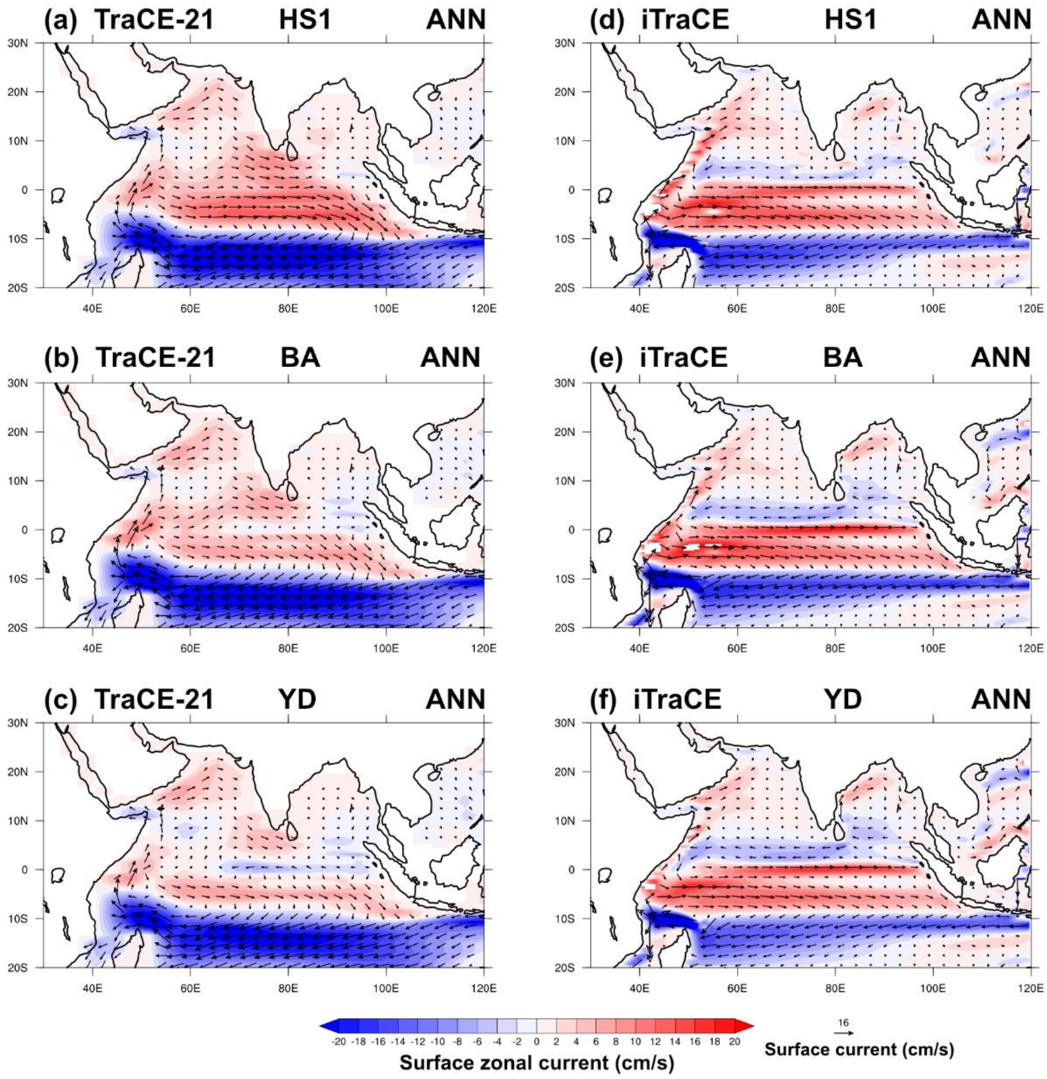

Fig. S7 Surface currents (arrows) and zonal currents (colour shading) simulated in the TraCE-21 model for the annual mean of (a) HS1 (18-14.7 ka), (b) BA (14.7-12.9 ka), and (c) YD (12.5-11.5 ka) (Liu et al., 2009). (d-f) are the same as (a-c) but for iTraCE simulation (He, 2021; He et al., 2021).

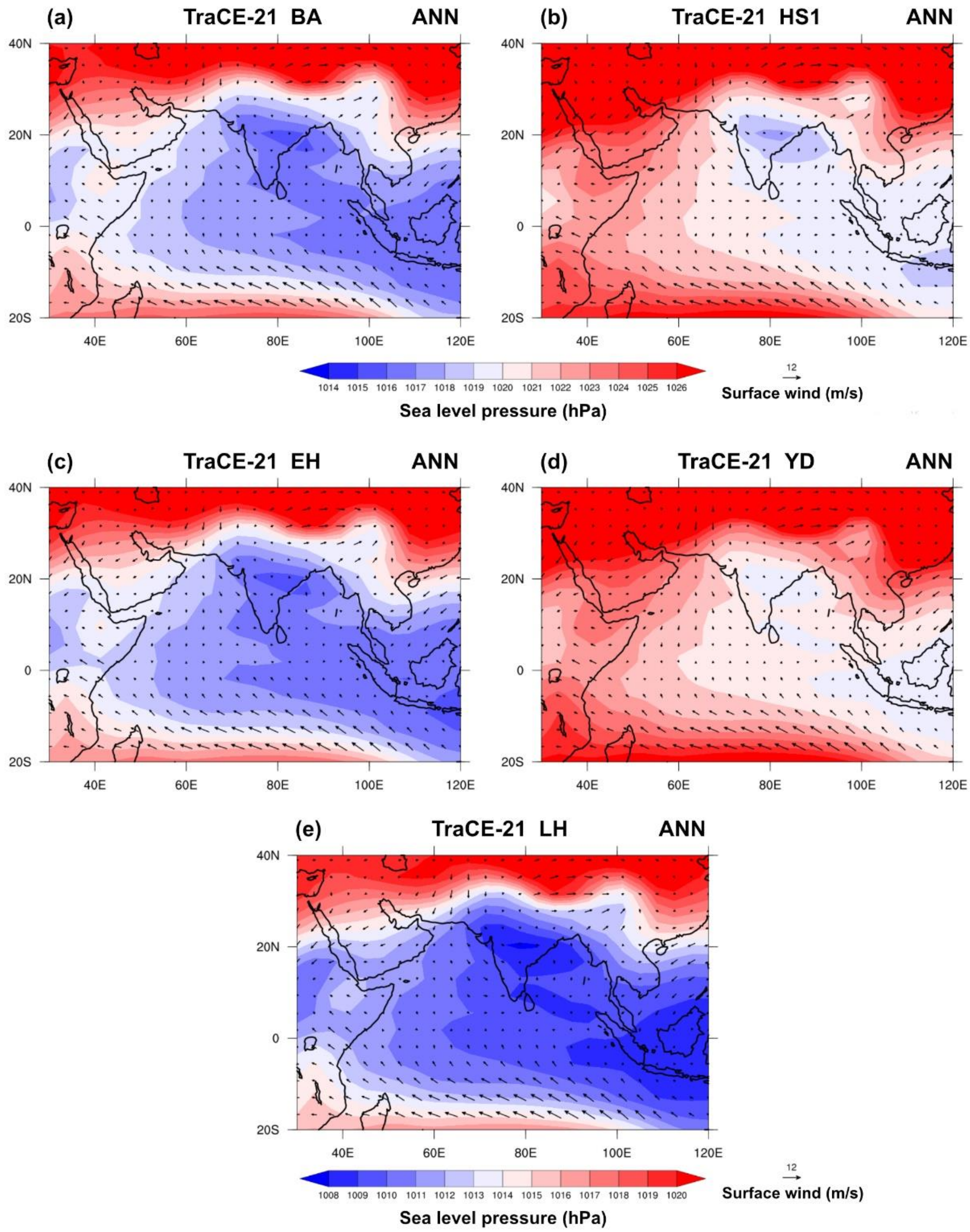

Fig. S8 Surface wind (arrows) and sea level pressure (colour shading) simulated in the TraCE-21 model for the annual mean of (a) BA (14.7-12.9 ka), (b) HS1 (18-14.7 ka), (c) EH (10-8 ka), (d) YD (12.5-11.5 ka), and (e) LH (2-0 ka) (Liu et al., 2009).

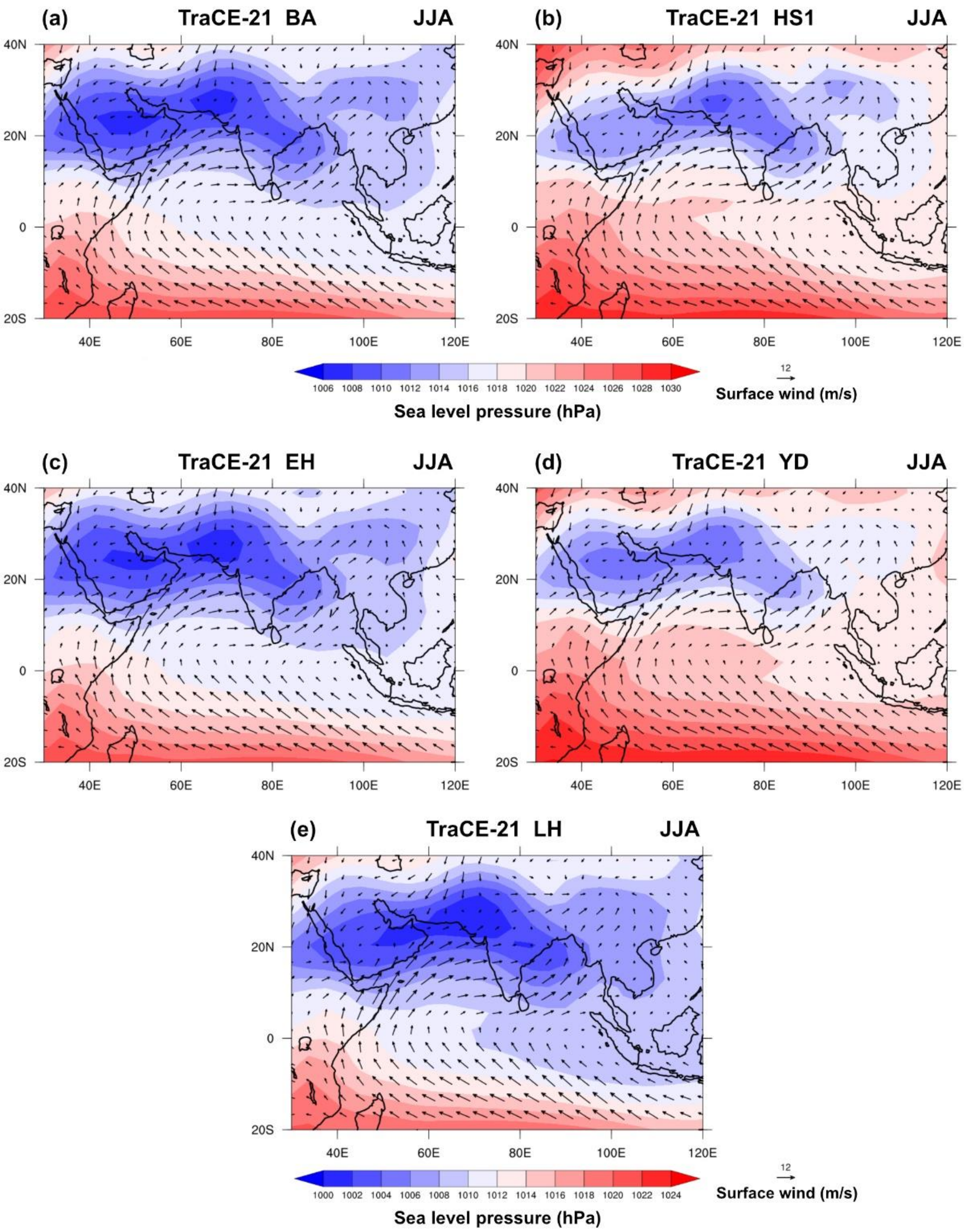

Fig. S9 The same as Fig. S8, but for summer (June, July, August) (Liu et al., 2009).

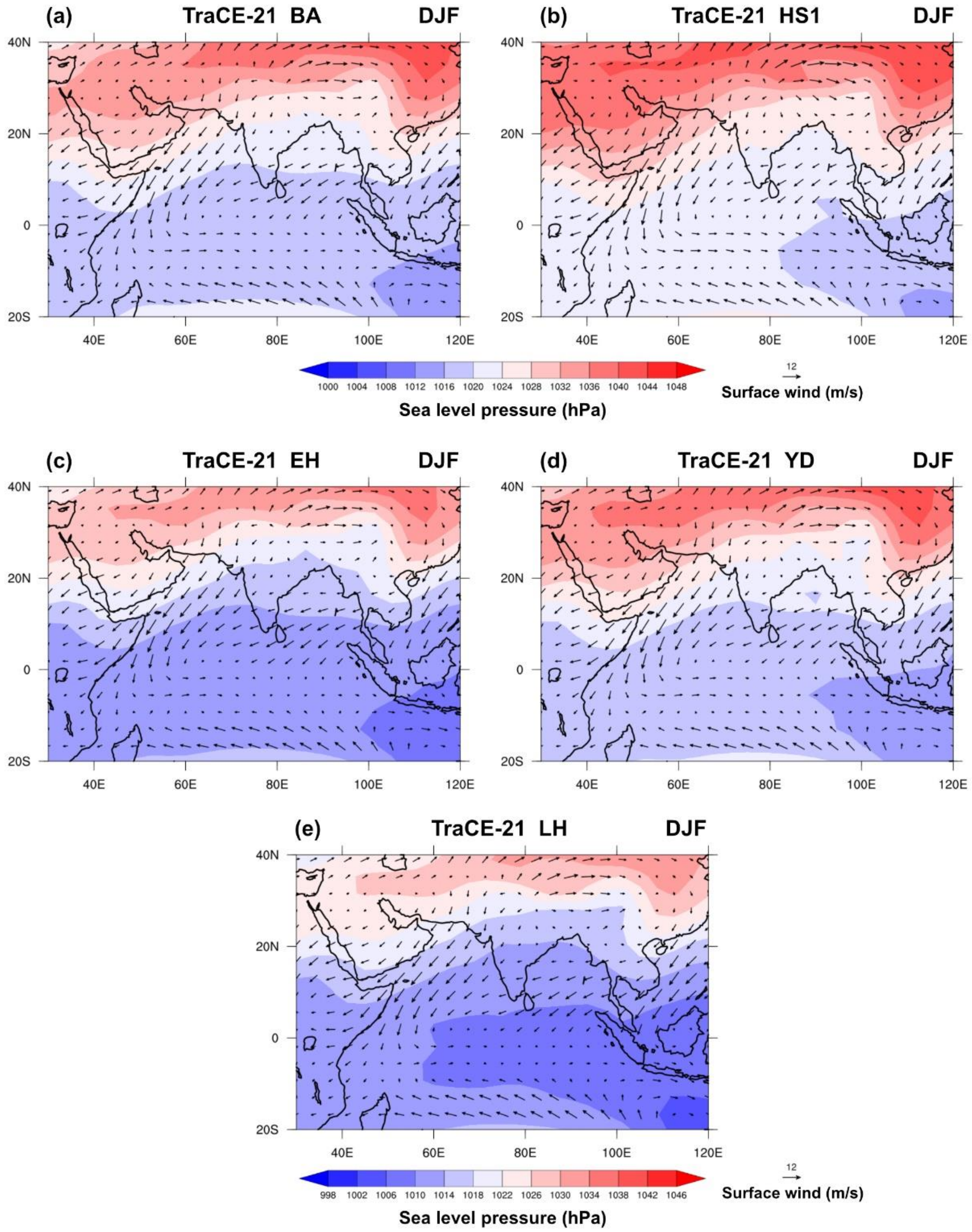

Fig. S10 The same as Fig. S8, but for winter (December, January, February) (Liu et al., 2009).

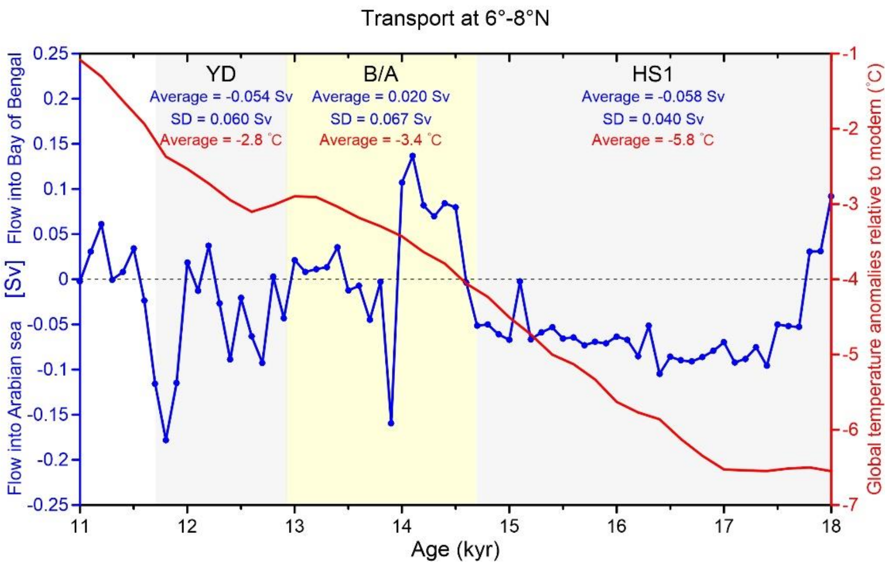

Fig. S11 Left panel shows the deglacial time series of zonal transport at 6-8°N, 77°E in the upper 100 m, derived from the iTraCE model (He, 2021; He et al., 2021). Positive values indicate an eastward flow into the Bay of Bengal, while negative values represent a westward flow into the Arabian Sea. Right panel shows global temperature anomalies relative to the modern, calculated from palaeoclimate data assimilation (Osman et al., 2021). The iTrace model shows that the net flows during HS1 (-0.058 Sv) and the YD (-0.054 Sv) are similar in direction (flows into the Arabian Sea) and amplitude, which is distinct compared to the B/A period (+0.020 Sv; flows into the Bay of Bengal). However, the intensity of water exchange (inferred from the variability) is similar between the B/A (0.067 Sv) and the YD (0.060 Sv), which are greater than during HS1 (0.040 Sv). From the cold HS1 to the BA and YD periods, with the increase of global temperature, the modelled intensity of water exchange increases, but the net effect of water exchange does not increase significantly.

Supplementary References

Bassinot, F., Marzin, C., Braconnot, P., Marti, O., Mathien-Blard, E., Lombard, F., Bopp, L., 2011. Holocene evolution of summer winds and marine productivity in the tropical Indian Ocean in response to insolation forcing: data-model comparison. Climate of the Past 7, 815-829.

He, C., 2021. Deciphering the deglacial evolution of water isotope and climate in the Northern Hemisphere. The Ohio State University.

He, C., Liu, Z., Otto-Bliesner, B., Brady, E., Zhu, C., Tomas, R., Clark, P., Zhu, J., Jahn, A., Gu, S., 2021. Hydroclimate footprint of pan-Asian monsoon water isotope during the last deglaciation. Science Advances 7, eabe2611.

Liu, Z., Otto-Bliesner, B., He, F., Brady, E., Tomas, R., Clark, P., Carlson, A., Lynch-Stieglitz, J., Curry, W., Brook, E., 2009. Transient simulation of last deglaciation with a new mechanism for Bølling-Allerød warming. science 325, 310-314.

Ma, R., Sépulcre, S., Bassinot, F., Haurine, F., Tisnérat-Laborde, N., Colin, C., 2020. North Indian Ocean Circulation Since the Last Deglaciation as Inferred From New Elemental Ratio Records for Benthic Foraminifera Hoeglundina elegans. Paleoceanography and Paleoclimatology 35.

Osman, M.B., Tierney, J.E., Zhu, J., Tardif, R., Hakim, G.J., King, J., Poulsen, C.J., 2021. Globally resolved surface temperatures since the Last Glacial Maximum. Nature 599, 239-244.